Non-exhaust particle emissions under various driving conditions: Implications for sustainable mobility

A. Beji, Karine Deboudt, S. Khardi, B. Muresan, Pascal Flament, Marc Fourmentin, L. Lumière

Non-exhaust particle emissions under various driving conditions: Implications for sustainable mobility

A. Beji[1], K. Deboudt[2], S. Khardi[1], B. Muresan[1], P. Flament[2], M. Fourmentin[2], L. Lumière[1]

[1)] The French Institute of Science and Technology for Transport, Development and Networks (IFSTTAR-EASE). University of Lyon (France)

[2)] Laboratoire de Physico-Chimie de l'Atmosphère (LPCA), Université du Littoral Côte d'Opale (ULCO), 59140 Dunkerque, France

Corresponding author

Email: asmabejii@gmail.com / asma.beji@ifsttar.fr
Postal address: 25 avenue François Mitterrand, 69500 Bron, Lyon, France
Phone: +33 (0)7 69 96 74 04

Keywords: Non-exhaust emissions; brake wear particles; tire-road contact particles; size distribution; chemical composition; air quality

Highlights

- The mass of non-exhaust particles (NEP) is distributed between the accumulation and coarse modes.
- The number concentration of NEP is shared between the nucleation and accumulation modes.
- Brake wear particle emissions are highly dependent on brake pad temperature.
- Tire-road contact emissions are determined by vehicle speed, acceleration and deceleration.
- The chemical composition and shapes of non-exhaust particles differ according to the size modes.

Graphical abstract

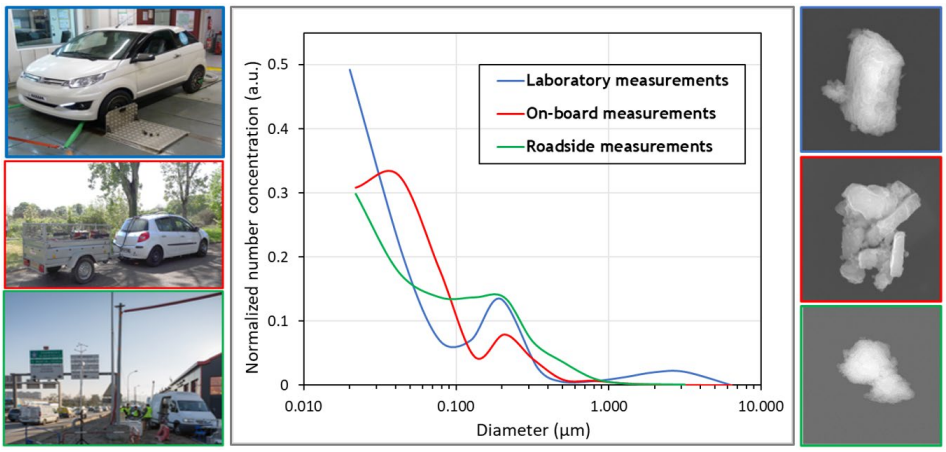

Abstract

Non-exhaust particle (NEP) emissions from road traffic contribute significantly to Particulate Matter (PM) pollution in urban areas. The primary objective herein is to develop the knowledge required to move toward more sustainable mobility. NEP emissions are studied by means of complementary experiments on chassis dynamometers, on test tracks and at the roadside. Laboratory tests demonstrate that brake wear particles (BWP) emissions can change with braking force and frequency. A brake pad temperature threshold exists, above which the rate of ultrafine particle emissions is quite high. Below this threshold, the BWP emissions are dominant in the accumulation and coarse modes. Test track measurements have demonstrated that tire-road contact particle (TRCP) emissions considerably modify the atmospheric PM background especially for the supermicron fraction. Their number size distribution highlighted an ultrafine and accumulation modes centered at about 40 nm and 200 nm, respectively. The TRCP level increases with vehicle speed and during the acceleration and deceleration phases. Roadside measurements in the urban environment confirm the presence of NEP in significant proportions, in both the accumulation and coarse modes. The chemical composition of NEP differs depending on the size mode: BWP mainly stem from the degradation of brake pad lining materials, while TRCP are a mixture of tire tread wear and re-suspended dust. The presence of Fe-rich particles nevertheless serves as a good indicator of their contribution to PM at the roadside. Lastly, in considering the parameters influencing NEP emissions, a series of recommendations are offered in order to achieve a more sustainable mobility.

1. Introduction

Traffic emissions have been responsible for air quality degradation for many years. Atmospheric Particulate Matter (PM) has been cited as causing some 430,000 premature deaths per year in Europe (European Environment Agency, 2015), and road traffic contributes significantly to their emissions, particularly in urban areas (Padoan and Amato, 2018). Ultrafine particles (in the nanometer size range) have particularly harmful effects on human health, by virtue of penetrating into the deep lung (Stone et al., 2017) and blood vascular system (Geiser and Kreyling, 2010), thereby increasing respiratory and cardiovascular morbidity, as well as lung cancer mortality through the mechanisms of oxidative stress and inflammation (Pope et al., 2002; Sun et al., 2010; Valavanidis et al., 2008).

Traffic-related particle emissions can be separated into exhaust emissions, resulting from incomplete fuel combustion and lubricant volatilization during the combustion procedure (Vouitsis et al., 2009), and non-exhaust emissions produced by brakes, tire and road surface wear, or by road dust resuspension (Thorpe and Harrison, 2008). Depending on the environment under consideration, exhaust and non-exhaust sources can contribute almost equally to total particle emissions from traffic (Harrison et al., 2001; Querol et al., 2004; Bukowiecki et al., 2010). However, as exhaust emissions controls have become more stringent, the relative contribution of non-exhaust emissions has increased commensurately (Kousoulidou et al., 2008; Van der Gon et al., 2013; Amato et al., 2014) and may now dominate in $PM_{2.5}$ (i.e. particles with an equivalent aerodynamic diameter < 2.5 μm) (Lawrence et al., 2016). These non-exhaust particles (NEP) have various sizes, shapes and chemical compositions (Grigoratos and Martini, 2014), depending on their origin (brake wear, tire wear, road surface wear, resuspension) or source-intrinsic parameters (e.g. brake and tire type, pavement texture).

72 The most abundant non-exhaust source is often assumed to be brake wear (Kwak *et* al., 2013;
73 Grigoratos and Martini, 2015), with a contribution of up to 55% by wt. of the non-exhaust
74 PM_{10} emissions near a major road in London (Harrison et al., 2012). Brake wear particle (BWP)
75 emissions depend on many factors, including: a) the type of brake pad (low metallic, semi-
76 metallic, non-asbestos organic pads), more specifically the lining material; b) the type of brake
77 assembly (drum brakes, disc brakes); and c) the vehicle operating conditions, e.g. initial speed,
78 deceleration and braking force (Garg *et* al., 2000; Hagino *et al.*, 2016, 2015; Iijima *et al.*, 2008,
79 2007; Sanders *et al.*, 2003).

80 The emissions of tire-road contact particles (TRCP) constitutes another major NEP source
81 (Kwak *et* al., 2013; Grigoratos and Martini, 2015), including the resuspension of road dust as
82 well as the wear of both tires and road surfacing materials. These emissions are likely to
83 change as a result of many factors, such as meteorological and traffic conditions, ambient
84 particulate pollution, driving style, variations in tire composition and texture, and road surface
85 characteristics (Lowne, 1970; Etyemezian et al., 2003; Dahl et al., 2006; Gustafsson et al.,
86 2008; Hussein et al., 2008; Pirjola et al., 2010; Sjödin et al., 2010; Grigoratos et al., 2018; Park
87 et al., 2018).

88 All these NEP are found not only in the coarse and fine fractions, but also in the ultrafine size
89 range (< 100 nm) (Dahl *et al.*, 2006; Mathissen *et al.*, 2011; Sjödin *et al.*, 2010), particularly at
90 high braking forces (Garg *et al.*, 2000; Mathissen *et al.*, 2011; Wahlström *et al.*, 2010b). Several
91 difficulties arise however when studying NEP due to a lack of standardized sampling
92 procedures and measurement techniques, which leads to non-comparable results (Grigoratos
93 and Martini, 2015). Moreover, many studies have focused on BWP emissions, whereas those
94 targeting TRCP emissions are relatively scarce due to the high contribution of resuspended

95 road dust, hence complicating application of the measurement and sampling methodologies
96 (Grigoratos and Martini, 2014; Foitzik et al., 2018).

97 In this context, our initial goal is to determine the physical and chemical nature of BWP and
98 TRCP, by means of implementing similar sampling and measurement methodologies that yield
99 comparable results on the coarse (1 µm < d < 10 µm), fine (100 nm < d < 1 µm) and ultrafine
100 (d < 100 nm) fractions. NEP emissions can be measured in different ways, namely: in the
101 laboratory under controlled testing conditions (Pelkmans and Debal, 2006; Hagino *et al.*, 2016;
102 Park *et al.*, 2018), on-board under semi-controlled testing conditions, and along the roadside
103 by integrating the PM emissions from a wide array of vehicles and under different traffic
104 conditions (Kwak *et al.*, 2014; Q. Zhang *et al.*, 2017). An original aspect of this work is studying
105 NEP emissions under these three test conditions so as to draw conclusions on particle
106 identification in various environments. BWP emissions have been studied by laboratory tests
107 conducted on a chassis dynamometer using a common car of the French fleet, which entailed
108 extracting new braking profiles from the ARTEMIS European driving cycles (André, 2004) and
109 considering different parameters like vehicle speed and brake pad temperature. On-board
110 measurements have been carried out on a test track to investigate TRCP emissions collected
111 at the rear of a wheel, in considering a range of driving conditions and distances from the
112 emission area. Lastly, roadside measurements, along a major French highway, allowed
113 characterizing NEP in an actual urban environment and comparing them with previous
114 findings under controlled and semi-controlled test conditions. In conclusion, through similar
115 sampling / measurement methods and complementary test conditions, the factors influencing
116 NEP characteristics are discussed and recommendations proposed in order to improve road
117 mobility within the framework of sustainable development.
118

2. Materials and methods

2.1 Instrumentation

Particle size distributions were acquired by means of real-time measurements using three different instruments: an Electrical Low Pressure Impactor (ELPI™), a Fast Mobility Particulate Sizer (FMPS™), and an Optical Particle Counter (OPC Grimm™). The data are presented in this study as concentrations normalized by the integral of the particle counts. The ELPI™ (Dekati™, ref. Classic ELPI™) measures the number size distribution for particles with an aerodynamic diameter between 7 nm and 10 µm, at a time step of 1 s. This device operates at a flow rate of 10 $L.min^{-1}$, with 12 size channels. For additional measurements of the ultrafine fraction (< 100 nm), the FMPS™ (TSI™, ref. 3091) was used to measure electrical mobility diameters between 5.6 nm and 560 nm, at a time resolution of 1 s and a 32-channel size resolution; this instrument is equipped with a cyclone head (50% cut-off aerodynamic diameter = 1 µm) and operates at a sampled air flow rate of 10 $L.min^{-1}$ and a sheath air flow rate of 40 $L.min^{-1}$. It relies on an electrical mobility measurement technique associated with a low-noise electrometer for particle detection. For these two particle sizers, mass size distributions are calculated from the number size distribution, in considering the particles to be spheres with a density of 1 $g.cm^{-3}$, not so far from the effective density of brake wear particles measured by Nosko and Olofsson (2017). Both devices had previously been calibrated by their manufacturers, and the similarity between normalized size distributions measured in parallel has been verified (Figure S1). The main modes are well coinciding for the two measurements although there is an apparent overestimation of particle counts in the nano-size range of ELPI, and therefore an underestimation of larger ones, which has already been reported and attributed to particle bounce (Virtanen et al., 2010; Leskinen et al., 2012). An Optical Particle Counter (OPC Grimm™, ref. EDM 1.108) is introduced to probe, on a complementary basis,

the accumulation and coarse mode particles. This device outputs real-time measurements of particles with an optical diameter lying between 0.35 and 22.5 µm, 15 size channels, a flow rate of 1.2 $L.min^{-1}$ and a step time of 6 s. The analyzer had been calibrated by its manufacturer using dolomite dust. Only number concentrations data from this instrumentation were used in this study.

For the chemical characterization step, atmospheric particles were collected on nickel Transmission Electron Microscopy (TEM) grids using a 3-stage cascade impactor (air flow: 28 $L.min^{-1}$) with nominal cut-off sizes (i.e. aerodynamic diameters at 50% of collection efficiency) of 10, 1.0 and 0.1 µm. Individual particle analyses were performed by Scanning Electron Microscopy with Energy-Dispersive X-ray spectrometry acquisition (SEM-EDX). Several hundred particles per impaction stage were detected and analyzed using a JEOL 7100F FEG-SEM equipped with a transmitted electron detector and three ultrathin-window (30 mm^2) energy-dispersive X-ray detectors (Bruker XFlash 6/30), enabling the analysis of elements with an atomic number higher than boron ($Z \geq 5$). Volatile and semi-volatile particles are likely to vaporize in the high vacuum environment of the SEM and are not observed. Therefore, the data from the SEM-EDX are only for non-volatile metallic constituents. Spectral acquisitions were performed at 15 kV, 300 pA for 20 s. The resulting large databases (particle size, morphological parameters *i.e.* particle projected area and Feret diameters, and elemental composition) were then statistically analyzed by means of Hierarchical Ascending Classification (HCA), using the FactoMineR software, clustering particles with similar characteristics, i.e. of comparable origin.

2.2 Sampling and measurement strategy

BWP emissions were studied in the laboratory on a chassis dynamometer (presented in Supplementary Information - Figure S2). Measurements and sampling were conducted on the side of the vehicle, about 8 cm from the wheel, using a conical sampling head (46 cm in diameter) centered on the wheel rim. To obtain a cooling pattern similar to real-world conditions, the engine compartment was cooled by a blower discharging a large-diameter stream of air toward the vehicle, with a flow rate proportional to the speed of the roller. Considering this sampling design, collection aspiration efficiencies (η) were calculated using an empirical approach developed by (Baron and Willeke, 2001), in a turbulent regime ($Re>4\times10^3$) and where the sampling inlet is oriented at an angle θ with respect to the air streamlines, using Equation 1:

$$\eta = 1 + \left[\left(\frac{U_0}{U}\right) cos\theta - 1\right]\left[3Stk^{\sqrt{\frac{U}{U_0}}}\right] \qquad \textit{(Equation1)}$$

Where U = inlet velocity, U_0 = flow velocity in the free-stream, Stk = Stokes number (calculated for a particle density of 1g.cm^{-3}) and θ = angle between the sampling inlet and the air streamlines (θ =53° in our case). The calculated aspiration efficiencies (Table S 1) are higher than 90% whatever the particle size and the simulated vehicle speed. The ELPI is directly connected in the continuity of the sampling head outlet by an 80 cm antistatic tube, without bend, so the loss of particles during this path between the sampling head and the ELPI is negligible. In parallel, the FMPS is connected to the side of the sampling head, using two 90° bends. Nevertheless, the fraction penetration in the bent section calculated according to Baron and Willeke (2001) is higher than 99% for particle diameters smaller than 300 nm (high detection limit of FMPS). In conclusion, the collection efficiency of BWP is higher than 90% whatever the particle size (<10µm) and the particle concentrations were then not corrected for this loss.

188 To avoid contamination from exhaust emissions, the emissions were extracted at the tailpipe
189 and evacuated to the outside after filtration. Three braking profiles, derived from the ARTEMIS
190 (Assessment and Reliability of Transport Emission Models and Inventory Systems) driving
191 cycles (André, 2004), were created to facilitate the qualitative characterization of brake wear
192 particle emissions: urban (maximum speed = 50 $km.h^{-1}$), suburban (maximum speed = 70 $km.h^{-1}$),
193 and highway (maximum speed = 120 $km.h^{-1}$). These profiles were designed to be
194 representative of actual driving conditions in Europe (André, 2004), yet with the high braking
195 frequencies necessary to generate a sufficient amount of braking particles for sampling and
196 analysis (Khardi and Nuel, 2017). They were performed by a same person. For these
197 experiments, we used a light-duty vehicle (Renault Clio III, 1.6 i 16V, 111 hp, one of the most
198 widely sold models in France) which was equipped with semi-metallic brake pads (TRW 8200
199 432 336/ 32 336188 PES) and cast iron discs. Brake discs are traditionally made of grey cast
200 iron with a pearlitic matrix (Cueva et al., 2003). Semi-metallic brake pads were purchased on
201 the mass market and correspond to an intermediate price range. They are available in most
202 EU countries (MSR, 2019). The brake temperature was monitored using an infrared
203 temperature sensor (Texense, Ref: IRN2-V800-5-V2) positioned directly in front of the brake
204 pads, 3 cm from the pad/disc contact surface.

205 TRCP emissions (including the re-suspension of road dust and wear of both tires and the road
206 surface) were studied under semi-controlled conditions on a test track (2.3 km long; max.
207 speed: 140 $km.h^{-1}$). The road surface of the test track is consisting of semi-coarse (0/10)
208 asphalt concrete with medium macrotexture (0.82-1.25 mm texture depth) and microtexture
209 (skid resistance of 49.1-56.1) levels. The constituent rocks of the aggregates used in the
210 asphalt concrete include both igneous rocks of felsic composition (rhyolite) and
211 metamorphosed igneous rocks (gneiss). The chemical composition of these rocks is typically

70-77% silica (SiO_2), 11-13% alumina (Al_2O_3) and K, Na, Ca Fe and Mg as minor elements. The tests were conducted under dry weather conditions (T = 20-25°C with 50%-80% humidity) and without significant wind (< 20 $km.h^{-1}$). To preserve the same driving behavior throughout the testing campaign, the same pilot / co-pilot team was used. Vehicle data (speed, speed variations, engine parameters, etc.) were recorded at a frequency of 10 Hz regardless of driving conditions. A trailer containing the scientific instrumentation, including two power generators, was hitched. The inlet of the TRCP sampling probe was placed in the axis of the wheel 15 cm behind the tire and 7 cm from the ground (Figure S2).

As for the laboratory experiments on a chassis dynamometer, the collection aspiration efficiencies (η) were calculated using an empirical approach developed by (Baron and Willeke, 2001) using Equation 1 (θ =75° in this case). The calculated aspiration efficiencies (Table S 2) are close to 100% for submicron particles (i.e. for the large majority of particles by number) whatever the speed of the vehicle (including when the vehicle is still for background measurement). For coarser particles (5-10µm), these efficiencies are slightly less good, especially for 10µm particles (65.2% in average). However, the relative evolution of this efficiency for a particle size as a function of vehicle speed is ≈ 10%, which is relatively low, that is why experimental particle concentrations have not been corrected for the aspiration efficiency. The influence of tubing on measured number concentrations was investigated prior to the sampling campaigns. The tubing used to convoy particles is a 5m long antistatic hoze with an inner diameter of 8 mm. The data showed that the particle loss amounts to 1.5%/m and that it is homogeneously distributed between fine and coarse particles (between <1% and 3% variation in the ratio between fine and coarse concentrations). Therefore, the particle concentrations were not corrected for this loss.

Background concentrations were obtained when the vehicle was idle, facing the wind. To assess NEP dispersion, measurements were also performed at the edge of the test track using the same instrumentation. The sampling points were located at 0.45 and 3.0 m from the driving lane and 0.45 m from the ground. The vehicle was fitted with summer tires (Michelin™ Energy Saver, 185/60 R 15 88H) purchased in the mass market. They have asymmetrical structures with three straight grooves that run around the center of the silica-based rubber tread. The elemental composition of the tire surface essentially consisted of C and O. Si, S, Zn, Fe and Ca were present as other major elements, i.e. ca. (in wt.%): 14%, 5%, 4%, 2% and 2% of the remaining, respectively. Al, Na, Cl, K and Mg were present as trace elements (i.e. less than 2wt.% of the total, once C and O have been discarded) or concentrated in localized areas. The tire surface was mostly amorphous with Si or Fe-enriched spots or inclusions. The shapes of inclusions were varied, ranging from spherical to cylindrical or highly amorphous.

Additional measurements and sampling were carried out at the roadside, along the A43 motorway near Lyon, France. To provide a representative braking situation, the measurement site was located at the "Saint Quentin Fallavier" toll plaza, offering a traffic-influenced site (approx. 81,000 vehicles/day) exempt from industrial emissions with an urban atmospheric background. The instrumentation was set up in March 2017, downwind a few meters from the road, under the direct influence of road traffic emissions. Sampling and measurement heads were installed at the top of a 2-m high mast, so as to represent the air inhaled by humans. During this measurement campaign, the same instruments and sampling techniques used during laboratory and test track experiments were implemented, thus yielding comparable results.

3. Results and discussion

3.1 Brake wear particle (BWP) emissions

3.1.1 Particle size distribution, shape and chemical composition

The BWP size distribution is variable and may depend on many factors. The effect of repetitive braking with the same force during urban braking profiles was investigated first. Figure 1 shows the evolution of this number size distribution during two successive urban profiles (about 900 seconds of continuous braking events). During the first profile (Urban 1 section), a bimodal distribution is observed with an accumulation peak centered at approx. 200 nm and a coarse peak at 2 µm. The accumulation mode is most certainly generated by mechanical friction, while coagulation processes result in the coarse mode formation. Consequently, this coarse mode is in all likelihood essentially formed by agglomerated wear particles. As braking events accumulate, the particle size distribution evolves into an additional emission of ultrafine particles (Figure 1, Urban 2.A section) and ultimately results at the end of the second profile (Urban 2.B section) in a unimodal distribution with a peak at a diameter less than 30 nm. Nanoparticle emissions were already observed when increasing the braking force at high vehicle speeds (Namgung *et al.*, 2016, 2017), but not with a constant braking force. Continuous braking events produce an increase in the friction surface temperature, as indicated by the increase in brake pad temperature (Figure 1). At a threshold temperature (about 250°C), the dual processes of brake pad thermal degradation and volatilization occur, and it can reasonably be assumed that this sequence leads to the abundant formation of nanoparticles by nucleation and condensation processes. This threshold temperature, associated with a significant change in BWP size distribution, has been confirmed for the three braking profiles studied in the next section and most likely depends on both the brake pad characteristics and temperature measurement techniques (Nosko and Olofsson, 2017).

The chemical composition of braking systems provides a good indication of the origin and formation processes of all these brake wear particles. Brake pads have a complex chemical composition that drastically varies depending on market price and manufacturer (Von Uexküll et al., 2005). The great diversity of pad compositions has already been highlighted in the literature, although certain elements considered as tracers for brake wear such as iron, copper or barium are more often mentioned (Garg et al., 2000; Sanders et al., 2003; Birmili et al., 2006; Thorpe and Harrison, 2008; Wahlström et al., 2010a; Pant and Harrison, 2013; Grigoratos and Martini, 2014; Hagino et al., 2016). Elemental maps of the brake pads used in our experiments have underscored the heterogeneous elemental distribution at the micrometric scale (Figure S3): some areas feature iron-rich components, while others are mainly composed of carbonaceous materials or mixed carbonaceous/metal agglomerates (C, O, Al, Si, S, Fe, Cu, etc.). This elemental distribution heterogeneity within the pad will probably generate a wide diversity of BWP, depending on the formation mechanism and pad area involved.

The cluster analyses from SEM-EDX data result in 7 clusters for BWP, whose names start by BW (Table 1). As expected, the individual BWP analysis shows a great diversity in chemical composition depending on the size modes considered. For the coarse mode, most BWP (BW-C3 type, with a relative abundance of P = 76%) form a complex mixture of carbon, oxygen and iron, with copper also being contained to a lesser extent and aluminum and silicon as minor elements. Generated by friction mechanisms and aggregation processes, these particles display Cu contents comparable to brake pads (i.e. 6.4% vs. 5.3%, respectively) as well as an agglomerated shape (see Figure 2). 17% of coarse particles (BW-C4 type) are iron-rich but do not contain copper. The absence of iron concomitants coupled with a carbon deficit would suggest disc wear as their likely source. Lastly, a small proportion of particles from this coarse

306 mode is carbonaceous particles also containing both iron and copper (BW-C1, P = 5%), or
307 particles containing in Al (BW-C2, P = 2%). This would reflect either an origin to the carbon-
308 based materials of the brake pads (including graphite, rubber and organic fibers) or, more
309 rarely, vermiculite and other inclusions enriched with aluminum and iron. For the
310 accumulation mode, most BWP (BW-A2 and BW-A3, P = 71%) are carbonaceous particles also
311 containing iron to a varying extent (10.3 to 23.4 wt. %) and copper in a less extent. They also
312 contain aluminum and silicon as minor elements. Their chemical compositions, which are
313 quite similar to those of the brake pads introduced, exclude a brake disc origin and are nearly
314 exclusively composed of iron. In addition, 29% of BWP from this accumulation mode (BW-A1,
315 Table 1) are carbonaceous, while containing nitrogen and sulfur as minor elements. Mainly
316 associated with a spherical shape (Figure 2), they probably stem from the degradation of the
317 carbonaceous areas of brake pads. BWP of the nucleation mode (< 100 nm), formed from
318 gaseous precursors, are too small to emit a signal detectable by SEM-EDX; however, when
319 considering the chemical composition of brake pads and discs, it can reasonably be assumed
320 that the majority of these BWP are carbonaceous, with carbon being among the less refractory
321 elements in braking systems. A significant fraction of these nanometric particles might also be
322 metal-rich (Liati *et al.*, 2019).

323 All these data from a vehicle equipped with semi-metallic brake pads clearly show that BWP
324 are primarily the result of brake pad degradation (*i.e.* chemical and mechanical breakdowns)
325 and not due to disc wear, except for a small fraction (17%) of coarse particles. Most BWP
326 contain Fe (Table 1), hence iron, as a major element at the particle scale, can be considered
327 as a tracer for BWP in the absence of other anthropogenic sources for this element. In the
328 case of semi-metallic and non-asbestos organic brake linings, iron powder and steel wool are
329 the major sources of iron (Thorpe and Harrison, 2008). For vehicles equipped with low-

metallic brake pads, the brake disc or drum may be the main contributors of Fe-containing particle emissions (Sanders *et al.*, 2003). In this latter case, Hulskotte *et al.* (2014) found that 70% of brake wear originates from the discs and only 30% from brake pads. Several other elements are proposed in the literature as tracers for BWP, e.g. antimony, barium, lead or zinc (Iijima et al., 2007; Charron et al., 2019). Their identification requires more sensitive yet global analytical techniques, which prove to be ineffective for individual particle analysis.

3.1.2 Influence of braking force and brake pad temperature on BWP emissions

The effect of braking intensity on BWP emissions has been studied using three driving profiles that differ according to the braking forces applied by the driver (urban, suburban and highway, see Figure S4), associated with maximum speeds of 50, 90 and 120 $km.h^{-1}$, respectively. Figures 3a, 3b and 3c show the temporal evolution of the size distribution of BWP emissions across various time intervals after the starting point of each test profile. These real-time measurements of number concentrations indicate that BWP emissions are not systematic for each brake use, and peak emissions are intermittently observed. PM resulting from brake wear likely occurs mainly as condensed nuclei and growing particles that partially stick to the available surfaces, including the disc (Augsburg *et al.*, 2011). This freshly-generated fraction could either be discharged by the air stream used for cooling the braking system or trapped for an indefinite period of time, thus explaining sporadic separation from the braking system surface. Regardless of braking profile, the BWP size distribution is similar with a highly dominant mode centered at 200 nm and a second highly tenuous mode centered at 10 nm. Nevertheless, the BWP concentration clearly depends on the braking profile being applied. On average, between 200 and 300 s after the braking profile starting point, number concentrations of $2.7 \cdot 10^3$, $2.0 \cdot 10^4$, and $1.0 \cdot 10^5$ cm^{-3} were observed for the urban, suburban

and highway profiles, respectively. In sum, stronger braking forces lead to the generation of BWP with the same mean size (near 200 nm), yet in higher quantities.

Brake pad temperatures corresponding to the size distributions presented in Figures 3a, 3b and 3c are on average 120°, 170° and 220°C, respectively. These temperatures, typically encountered during normal braking under actual driving conditions (Garg *et al.*, 2000), lie below the point where nanometric particle generation is observed. However, if the number of times applying the brakes were to be drastically increased, like during the highway type experiment, then the temperature would increase to 400°C after 500-600 s and the BWP size distribution would change significantly (Figure 3d), with a strong emission of nanoparticles centered around 10 nm. Previous studies also reported that the size distribution when braking occurs at a vehicle speed of around 120 $km.h^{-1}$ displays a maximum at approx. 11 nm (Mathissen et al., 2011; Kwak et al., 2014). Although such temperatures are not commonly observed during actual driving, these results do confirm our previous assumption of a brake pad temperature threshold above which ultrafine BWP (core mode centered at about 10 nm) are generated in great numbers regardless of the braking force. This threshold differs according to the braking profile under consideration and, therefore, according to the braking forces applied: it equals approx. 250°, 300° and 350°C for urban, suburban and motorway profiles, respectively (Figure S5). Of course, these thresholds probably depend on the type and composition of the brake pads used. These values are therefore specific to a semi-metallic brake pad and with a temperature measurement methodology close to the one used here.

3.2 Tire-road contact particles (TRCP)

3.2.1 Particle size distribution, shape and chemical composition

376 The formation of ultrafine TRCP has already been reported in the literature, with diameters of
377 30-60 nm and less than 30 nm for studded and non-studded tires, respectively (Dahl *et al.*,
378 2006; Å. Sjödin *et al.*, 2010; Foitzik *et al.*, 2018), along with the emission of a coarse fraction
379 (Kwak *et al.*, 2013; Å. Sjödin *et al.*, 2010; Hussein *et al.*, 2008). In this study, the vehicle used
380 was fitted with summer tires. At a constant vehicle speed anywhere in the range from 50 to
381 90 $km.h^{-1}$, the TRCP number size distribution after background removal is bimodal (Fig. 4a),
382 with a distinct ultrafine mode centered around 30-60 nm and a more minor accumulation
383 mode centered around 200 nm. The mass size distribution is also bimodal, with an
384 accumulation mode centered at 300 nm and a major coarse mode centered at 2-4 µm (Fig.
385 4a). The particle diameters at which these emission modes are centered do not depend on
386 vehicle speed, but their relative proportional values vary with it (Fig. 4b). The TRCP-to-
387 background number concentration ratio is close to one for submicron particles (on average,
388 1.44 and 1.65 for the 10 - 100 nm and 100 nm - 1 µm size ranges, respectively), and it only
389 increases slightly with vehicle speed. These TRCP emissions consequently give rise to just a
390 limited change in the submicron fraction of the atmospheric aerosol at the rear of the wheel
391 for ambient concentrations commonly found in European urban environments (7,100
392 $particles.cm^{-3}$ including a very large fraction of ultrafine particles and 25-30 $\mu g.cm^{-3}$ dominated
393 by particles from the accumulation and coarse modes). In contrast, the TRCP-to-background
394 number concentration ratio is higher for the 1-10 µm size range (Fig. 4b) and increases
395 substantially with vehicle speed, up to approx. 5.7 at 90 $km.h^{-1}$. This finding clearly highlights
396 an increase in the proportion of coarse TRCP at high speed, i.e. with more turbulent air
397 streams and shear stresses developing at the tire-road pavement interface. A significant
398 change thus occurs in the supermicron fraction of the wheel rear atmospheric aerosol due to
399 TRCP emissions.

The evolution of the TRCP-to-background number concentration ratios vs. vehicle speed (α, in $km.h^{-1}$) can be fit in the 0 - 90 $km.h^{-1}$ range by use of an exponential law, as follows:

$$\frac{TRCP}{Bkgd} = 1 + \exp\left(A\alpha\right) \qquad \textit{(Equation2)}$$

Where Bkgd is the background number concentration for the day of measurements and "A" an empirical proportionality factor. The following values with the associated coefficient of determination (r^2) were obtained for the different size ranges: $(A,r^2)_{10\text{-}100nm}$ = (0.0050, 0.92), $(A,r^2)_{100nm\text{-}1\mu m}$ = (0.0070, 0.93), $(A, r^2)_{1\text{-}10\mu m}$ = (0.0204, 0.99), the latter being semi-quantitative considering the lower collection efficiency of particles above 5µm (Table S 1). This result and previous research (Etyemezian et al., 2003; Dahl et al., 2006; Hussein et al., 2008; Gustafsson et al., 2008; Foitzik et al., 2018) serve to confirm that driving conditions, including speed, should not be ignored in the strategies implemented to reduce NEP emissions from road traffic.

The cluster analyses of data from SEM-EDX result in 8 clusters for TRCP, whose names start by TRC (Table 1). As observed for BWP, the TRCP chemical composition differs by size mode. Accumulation mode particles were mostly carbonaceous, containing silicon as a minor element (64% / TRC-A2). 18% of them (TRC-A1) were mixed carbonaceous-aluminosilicate particles and 19% (TRC-A3) were mixed carbonaceous/Fe-rich particles, which is consistent with a mixture of road surface dust and tire components. Carbon is the main component of asphalt binders but also of tire treads. Silicon, found in high quantities in some tire formulations, is used in tire reinforcing filler materials (up to 66% in superficial micrometric fibers). These materials also include iron and zinc as minor components (Adachi and Tainosho, 2004; Camatini *et al.*, 2001; Gustafsson *et al.*, 2008). The relative stability of zinc content in

422 tires makes this trace element a common tracer of tire wear emissions (Councell *et al.*, 2004;
423 Davis *et al.*, 2001), but it is not sufficiently present in the TRCP to be detectable at the particle
424 scale by SEM-EDX. For the coarse mode, 40% of TRCP were mixed carbonaceous/salt
425 (containing NaCl) particles, most likely re-suspended sea-salt particles (Table 1 / TRC-C5)
426 which are expected due to the presence of the Atlantic Ocean coast 20 km southwest of the
427 test track and predominant southwest winds during our experiments. Approximately 20% of
428 TRCP were aluminosilicates containing K and Na as minor elements (TRC-C1), which are
429 terrigenous particles stemming from dust resuspension. 14% of coarse TRCP (TRC-C4) consist
430 of aluminosilicate particles that also contain Na, Mg, Ca and Fe. The iron content in 19% of
431 TRCP (TRC-C3) (35.5 wt. %) is too high to correspond to mineral dust, hence these particles
432 are probably iron-rich from brake or tire wear potentially mixed with terrigenous dust on the
433 road surface (the iron content of the metal inclusions apparent on the surface of the tire and
434 brake pads exceed 65% and 90% by mass, respectively). Pavements normally have a rocky
435 ballast, which result in wear particles composed of minerals dominated by elements such as
436 Si, Ca, K, Al and Fe (Lindgren, 1996) as well as other minor components like titanium (from <
437 0.1% to 33%). All these observations suggest that a high proportion of coarse TRCP are re-
438 suspended particles.

439
440 ### 3.2.2 Influence of acceleration and deceleration on TRCP emissions

441 As traffic intensifies, both accelerations and decelerations can exert a significant impact on
442 TRCP emissions. As such, strong TRCP concentrations were recorded for both the
443 accumulation and coarse modes during acceleration/deceleration cycles (Figure 5). Although
444 the increase in TRCP-to-background number concentration ratios was close to that during the
445 mildest accelerations, these ratio values rapidly increased above 2.45 $m.s^{-2}$: TRCP

concentrations measured at 3.10 $m.s^{-2}$ exceeded by a factor of close to 12 those measured at 2.30 $m.s^{-2}$ (Figure 5). TRCP emissions were not constant during the accelerations: the strongest accelerations (i.e. > 2.50 $m.s^{-2}$) were actually characterized by an initial maximum in number concentrations containing all the previously identified modes (i.e. ultrafine, 55-60%; accumulation, 3-10%; and coarse, 10-15%), followed by a sudden and sharp increase in particles from the ultrafine mode (85-95% of total measured particles). This sequence resulted in significantly smaller mean diameters than those obtained for constant-speed driving or during small accelerations, i.e. < 100 nm vs. 150-340 nm, respectively. The pronounced increase in ultrafine mode level probably accounted for differing generation mechanisms, e.g. tire wear at higher temperature or associated with a more intense road dust fragmentation.

For decelerations, the TRCP concentration increased with both braking intensity (Kim and Lee, 2018; Lee *et al.*, 2013) and speed at the start of braking (i.e. with braking power) (Figure 5). For instance, at similar deceleration rates (6.9-7.0 m s^{-2}) experienced at initial speeds of 50 $km.h^{-1}$ and 110 $km.h^{-1}$, the TRCP-to-background number concentration ratios calculated over the 0.35-10 µm range rose by a factor of about 3, thus corresponding to a threefold increase in TRCP emissions since the background remains relatively constant during the tests. Unlike accelerations and despite the predominance of submicron particles, the proportion of coarse particles climbed significantly, from 16% to 33%.

Let's finally note that BWP emissions are most likely to account for a small proportion of TRCP concentrations: this is estimated from changes in the concentration ratio <1 µm to >1 µm to be around 10% between measurements at rear of the tire and a few centimeters downstream of the brake system. After emission, BWP are rapidly incorporated into the cloud of resuspended particles and then removed by the airflow downstream of the vehicle. However,

the calculated percentage is only a lower limit. It is, indeed, not currently possible to make a strict distinction between direct emissions of BWP and those resulting from resuspension.

In sum, compared to constant-speed traffic, accelerations and decelerations significantly raise TRCP and BWP emissions. Traffic fluidization should therefore be adopted as an imperative objective during measurement campaigns aimed at developing sustainable mobility.

3.2.3 Dispersion of TRCP at various distances from the driving lane

To assess the dispersion of BWP and TRCP, additional measurements were recorded at the edge of the test track, 0.45 and 3.0 m from the driving lane, thus from the TRCP measurement point when the vehicle passes in front of the roadside instrument. Measurements corresponding to the vehicle passing in front of the instrument (called "sample") were extracted and compared to the atmospheric background (i.e. measured near the test track when the vehicle is idle with its engine turned off). These "samples" incorporate the background, NEP (BWP+TRCP) and exhaust particle emissions. Interestingly, for ambient concentrations commonly found in European urban environments (i.e. 7,100 $\pm$ 800 particles cm^{-3}, or 25-30 µg m^{-3}), the sample-to-background concentration ratios recorded at 0.45 and 3.0 m from the edge of the test track (Figure 6) were close to one another and did not vary significantly with vehicle speed. For the coarse fraction (1-10 µm), whose contribution of fresh exhaust emissions can be considered negligible in light of their submicron size (Li *et al.*, 2018; Lu *et al.*, 2012), NEP emissions accounted for an average increase of 55% and 15% in the number concentration of background particles at 0.45 m and 3.0 m, respectively. In considering that there is no BWP emission at constant speed (i.e. without brake application), the decrease in the NEP so in the TRCP concentrations observed between the rear of the tire (Figure 4) and 0.45 m from the driving lane (Figure 6) demonstrates here that the TRCP were

largely removed from the immediate vicinity of the driving lane (i.e. 0.45m), most likely through deposition of the coarser particles and rapid dilution in incoming air during turbulent dispersion. The decrease in TRCP number concentration with increasing distance from the road is more pronounced at higher speeds: for the 1-10 µm fraction, the TRCP-to-background ratios were strongly correlated with vehicle speed (Figure 4), while the sample-to-background ratios at 0.45 m and 3.0 m from the driving lane remained for the most part unchanged (Figure 6). This finding underscores the increased turbulence in the mixing of air masses around the vehicle, thus resulting in higher dilution and dispersion rates, which ultimately counteract the TRCP concentration step-up in back of the wheel with vehicle speed. TRCP emissions from a single vehicle do not therefore contribute to a greater increase in PM level within the roadside atmosphere. However, a constant traffic flow would promote chronic impregnation of the roadside atmosphere with freshly emitted TRCP and/or more evolved particles (i.e. mixtures of exhaust and non-exhaust particles that have undergone one or more deposition, alteration and re-suspension cycles).

3.3. Implications for air quality in urban environments

To the best of our knowledge, no studies have sought to compare the micro-characteristics of particles collected both in an urban environment and during laboratory experiments conducted on brake wear and tire-road contact emissions. Many studies however have focused on ambient PM measurements in the urban environment, close to roadways, in identifying potentially high particulate levels from road traffic. The contribution of non-exhaust emissions to roadside PM concentrations, as generally evaluated from trace metals, is highly variable according to the studies, from a few to several tens of percent (Cahill et al., 2016; Charron et al., 2019; Jeong et al., 2019; Lawrence et al., 2016). This variability can be

explained by the distance from the roadside, with a reduction of up to about 40% of the particle number concentration at a distance of 10 m, but more likely by the driving mode, local topography and weather conditions (Fujitani *et al.*, 2012; Kumar *et al.*, 2014; Oakes *et al.*, 2016; X. Zhang *et al.*, 2017).

PM mass concentrations measured during our experiments at a toll plaza on a heavily-trafficked motorway, with stop-and-go traffic conditions, exhibit a large submicron particle fraction (PM1 counts for 75% of PM10). The mean PM_1, $PM_{2.5}$ and PM_{10} concentrations were of approx. 22.5 $\mu g.m^{-3}$, 26.7 $\mu g.m^{-3}$ and 30 $\mu g.m^{-3}$, respectively. These values are close to the local urban background measured by the air quality monitoring network over the same period at about 20 km away (daily mean $PM_{2.5}$ and PM_{10} values of 27 $\mu g.m^{-3}$ and 33 $\mu g.m^{-3}$, respectively). This finding demonstrates the relatively low impact of direct traffic emissions from the road adjacent to the measurement site on PM mass concentrations, as expected by our previous experiments on test tracks at variable distances from the driving lane (Section 3.2.3.). Another explanation lies in both the width of the toll plaza (some 120 m for 32 gates) so the far distance between the emission and measurement points and the smooth topography with no buildings in the near field, which favors higher dispersion of local emissions. Roadside studies systematically showed a rapid decrease in pollutant levels with increasing distance from the roadside (Cahill et al., 2016; Enroth et al., 2016; Oakes et al., 2016). The concentration gradient is variable and depends strongly from the air mass dynamics. For example, Enroth et al. (2016) observed half-decreases in PM1 concentration ranging from 3 m to 75 m from the highway depending on the environment considered, which can lead to roadside PM concentrations relatively close to those of the urban background. Thus, the PM collected here is considered to be representative of urban particulate matter,

whose overall emissions from the entire dense urban road network certainly make a significant contribution.

The number size distribution is bimodal (Figure S6) with one mode at a diameter less than 30 nm (nucleation mode) and another at 100-200 nm (accumulation mode). The finer mode corresponds to nanoparticles freshly formed from gaseous precursors, generally mainly consisting of volatile organic, nitrogen and sulfur compounds; it may stem from regional particle nucleation but also from traffic exhaust emissions or else include NEP (Agudelo-Castañeda et al., 2018; Enroth et al., 2016; Jeong et al., 2015). The mass size distribution is also bimodal (Figure S6) with maximum concentration around 0.4-0.6 µm and above 3 µm. The coarse mode, which is more abundant than the finer one, may include a significant proportion of NEP, which notably would fit with the non-exhaust coarse particles observed during our laboratory and test track experiments (Figure 1 and Figure 4) and has been reported in the literature (Harrison *et al.*, 2012).

In recognizing the absence of industrial iron sources at the regional scale, the presence of Fe-rich particles is a good indicator of the contribution of non-exhaust emissions to ambient PM levels in the urban environment, as already observed (Achad et al., 2013; Bucko et al., 2011; Charron et al., 2019; Sanderson et al., 2016; Weinbruch et al., 2014). The proportion of Fe-containing particles at the studied site is relatively high, i.e. around 60% of analyzed particles for the coarse fraction (aerodynamic diameter > 1 µm). This proportion is lower (by about 10% among the analyzed particles) for the submicron fraction, which is essentially composed of carbonaceous particles. These Fe-containing particles are basically iron oxide particles enriched to a various degree in carbon (Table S2); most of them also contain silicon in low amounts, owing to the NEP collected from brake wear and tire-road contact during our

563 experiments (Table 1). About 58% of the coarse Fe-containing particles (FeR-C1) consist
564 primarily of iron oxides, and only 23% of the coarse Fe-containing particles (FeR-C2) are
565 aluminosilicates, enriched in Ca and Fe (Table S2). All these coarse Fe-containing particles are
566 mostly angular and typically consist of aggregates, which suggests the presence of a friction
567 production mechanism. In addition, when normalized to C content, the chemical composition
568 of FeR-C1 and FeR-C2 particles approximates that of commercial brake pads with high (> 5%)
569 and low (< 5%) Fe content, respectively. Ba and/or Sb, also present in brake emissions
570 (Sanderson *et al.*, 2016; Gietl *et al.*, 2010; see Figure 7), are sometimes detected as minor
571 elements. In sum, Fe is a ubiquitous element in urban areas and, besides local sources (traffic,
572 home heating, waste incineration, etc.), the long-range transport of both mineral dust and
573 anthropogenic particles may contribute to Fe concentrations at the urban scale, especially for
574 fine and ultrafine particles. However, in considering Fe-rich particle abundance as an indicator
575 of the presence of NEP in the coarse PM fraction, our results suggest that for these
576 supermicron particles, non-exhaust emissions do make a significant contribution to PM levels
577 in urban environments.

578

579 ## 4. Conclusion and recommendations

580 In conclusion, the testing of three distinct environments (controlled in the laboratory, semi-
581 controlled with a test track and in an actual urban environment) using the same
582 instrumentation, sampling protocol and data processing methodology has made it possible to
583 obtain complementary results on NEP. To summarize, for urban and suburban driving
584 conditions, the emission of ultrafine BWP (< 100 nm) is low in comparison with particles
585 emitted in the 100-200 nm range (accumulation mode) and 2.5-4 µm range (coarse mode) due
586 to the limited increase in brake pad temperature. The elemental composition of these BWP

587 clearly indicates that over 70% of them are due to brake pad wear. Although tire and
588 pavement wear generates ultrafine particles, it is mainly the supermicron fraction of TRCP
589 emissions that alters the composition of the atmospheric background noise. Most TRCP
590 associated with the accumulation mode stem from tire wear, whereas a large proportion of
591 the coarse TRCP consist of re-suspended road dust, as well as more evolved particles
592 originating from the tire, brake and road surface wear. BWP and TRCP generated under
593 controlled and semi-controlled conditions have thus been extensively characterized;
594 moreover, particles with similar characteristics (size, morphology and chemical composition)
595 have been detected along the roadside, thereby highlighting the real impact of NEP on urban
596 air quality.

597 Information gleaned on the key parameters controlling NEP emissions can be used to issue
598 recommendations intended to reduce non-exhaust emissions and improve sustainable
599 mobility. Among the parameters tested, BWP emissions and TRCP levels markedly increase
600 with both speed and speed variations. Accordingly, limiting driving speeds to 70 km h^{-1} and/or
601 smoothing traffic flow would help reduce NEP emissions. This goal can be achieved without
602 any excessive investment, simply by means of various strategies typically implemented to
603 improve driving safety or reduce exhaust emissions (through speed limit monitoring, road
604 space rationing, congestion pricing, etc.). Eco-driving practices, combined with a dedicated
605 infrastructure that reasonably limits speed and both the intensity and frequency of speed
606 variations, are particularly able to reduce NEP levels in the near-road field.

607 TRCP emissions are conditioned locally by the degree of contamination and chemical
608 composition of the dust deposited on the pavement (including the recycling of exhaust and
609 non-exhaust emissions). This approach necessitates on-board and roadside devices capable of

detecting situations prone to non-exhaust emissions and warning drivers to adapt their speed. Moreover, given that the chemical composition of NEP is correlated with the composition of both brake pads and tires, making progress in the composition of these pads and in tire tread toward less toxic and more environmentally-friendly materials would be a positive step.

Acknowledgments

This study was funded by ADEME (French Environment and Energy Management Agency) through the "Physical Characterization of the Non-Exhaust Particle Emissions by Road Vehicles" project (or Captatus) (grant number: 1566C0016). In particular, the authors gratefully acknowledge L. Gagnepain with ADEME for fruitful scientific exchanges. Financial support has also been provided by the CaPPA project (Chemical and Physical Properties of the Atmosphere), which is funded by the French National Research Agency (ANR) through the PIA (Future Investment Program) under contract "ANR-11-LABX-0005-01", as backed by the "Hauts-de-France" Regional Council and European Regional Development Fund (ERDF). The authors would also like to thank the "Hauts-de-France" Region and the Ministry of Higher Education and Research (CPER IRenE), as well as the European Fund for Regional Economic Development, for their financial support.

The authors appreciate Atmo Auvergne-Rhône-Alpes, and notably Alexandre Thomasson, for assistance offered during field campaigns and for data provided from the French air quality monitoring network.

Also, special thanks are in order to P. Tassel, S. Serindat and P. Perret for their help in preparing the laboratory experiments, and to L. Suard, S. Louis, A. Guilloux and S. Buisson for their assistance in setting up the test track experiments and ensuring vehicle availability.

Lastly, we would like to thank the editor and reviewers for careful reading, and constructive comments and suggestions for our manuscript, as these comments helped us to improve this study.

References

Achad, M., Lopez, M.L., Palancar, G.G., Toselli, B.M., 2013. Retrieving the relative contribution of aerosol types from single particle analysis and radiation measurements and calculations: A comparison of two independent approaches. Journal of Aerosol Science 64, 11–23. https://doi.org/10.1016/j.jaerosci.2013.05.008

Adachi, K., Tainosho, Y., 2004. Characterization of heavy metal particles embedded in tire dust. Environment International 30, 1009–1017. https://doi.org/10.1016/j.envint.2004.04.004

Agudelo-Castañeda, D.M., Teixeira, E.C., Braga, M., Rolim, S.B.A., Silva, L.F.O., Beddows, D.C.S., Harrison, R.M., Querol, X., 2018. Cluster analysis of urban ultrafine particles size distributions. Atmospheric Pollution Research. https://doi.org/10.1016/j.apr.2018.06.006

Amato, F., Cassee, F.R., Denier van der Gon, H.A.C., Gehrig, R., Gustafsson, M., Hafner, W., Harrison, R.M., Jozwicka, M., Kelly, F.J., Moreno, T., Prevot, A.S.H., Schaap, M., Sunyer, J., Querol, X., 2014. Urban air quality: The challenge of traffic non-exhaust emissions. Journal of Hazardous Materials 275, 31–36. https://doi.org/10.1016/j.jhazmat.2014.04.053

André, M., 2004. The ARTEMIS European driving cycles for measuring car pollutant emissions. The Science of the Total Environment 334–335, 73–84. https://doi.org/10.1016/j.scitotenv.2004.04.070

Augsburg, K., Gramstat, S., Horn, R., Sachse, H., 2011. Measures Development for Brake Dust Emissions with Computational Fluid Dynamics and Particle Imaging Velocimetry (SAE Technical Paper No. 2011- 01–2345). SAE International, Warrendale, PA. https://doi.org/10.4271/2011-01-2345

Baron, P.A., Willeke, K., 2001. Aerosol measurement: principles, techniques, and applications. 2nd ed. (Book) | ETDEWEB [WWW Document]. URL https://www.osti.gov/etdeweb/biblio/20556104 (accessed 11.18.19).

Birmili, W., Allen, A.G., Bary, F., Harrison, R.M., 2006. Trace Metal Concentrations and Water Solubility in Size-Fractionated Atmospheric Particles and Influence of Road Traffic. Environmental Science & Technology 40, 1144–1153. https://doi.org/10.1021/es0486925

Bucko, M.S., Magiera, T., Johanson, B., Petrovsky, E., Pesonen, L.J., 2011. Identification of magnetic particulates in road dust accumulated on roadside snow using magnetic, geochemical and micro-morphological analyses. Environmental Pollution 159, 1266–1276. https://doi.org/10.1016/j.envpol.2011.01.030

Bukowiecki, N., Lienemann, P., Hill, M., Furger, M., Richard, A., Amato, F., Prévôt, A.S.H., Baltensperger, U., Buchmann, B., Gehrig, R., 2010. PM10 emission factors for non-exhaust particles generated by road traffic in an urban street canyon and along a freeway in Switzerland. Atmospheric Environment 44, 2330–2340. https://doi.org/10.1016/j.atmosenv.2010.03.039

Cahill, T.A., Barnes, D.E., Lawton, J.A., Miller, R., Spada, N., Willis, R.D., Kimbrough, S., 2016. Transition metals in coarse, fine, very fine and ultra-fine particles from an interstate highway transect near Detroit. Atmospheric Environment 145, 158–175. https://doi.org/10.1016/j.atmosenv.2016.09.023

Camatini, M., Crosta, G.F., Dolukhanyan, T., Sung, C., Giuliani, G., Corbetta, G.M., Cencetti, S., Regazzoni, C., 2001. Microcharacterization and identification of tire debris in heterogeneous laboratory and environmental specimens. Materials Characterization 46, 271–283. https://doi.org/10.1016/S1044-5803(00)00098-X

Charron, A., Polo-Rehn, L., Besombes, J.-L., Golly, B., Buisson, C., Chanut, H., Marchand, N., Guillaud, G., Jaffrezo, J.-L., 2019. Identification and quantification of particulate tracers of exhaust and

682 non-exhaust vehicle emissions. Atmospheric Chemistry and Physics 19, 5187–5207.
683 https://doi.org/10.5194/acp-19-5187-2019
684 Councell, T.B., Duckenfield, K.U., Landa, E.R., Callender, E., 2004. Tire-Wear Particles as a Source of
685 Zinc to the Environment. Environmental Science & Technology 38, 4206–4214.
686 https://doi.org/10.1021/es034631f
687 Cueva, G., Sinatora, A., Guesser, W.L., Tschiptschin, A.P., 2003. Wear resistance of cast irons used in
688 brake disc rotors. Wear. https://doi.org/10.1016/S0043-1648(03)00146-7
689 Dahl, A., Gharibi, A., Swietlicki, E., Gudmundsson, A., Bohgard, M., Ljungman, A., Blomqvist, G.,
690 Gustafsson, M., 2006. Traffic-generated emissions of ultrafine particles from pavement–tire
691 interface. Atmospheric Environment 40, 1314–1323.
692 https://doi.org/10.1016/j.atmosenv.2005.10.029
693 Davis, A.P., Shokouhian, M., Ni, S., 2001. Loading estimates of lead, copper, cadmium, and zinc in
694 urban runoff from specific sources. Chemosphere 44, 997–1009.
695 https://doi.org/10.1016/S0045-6535(00)00561-0
696 Enroth, J., Saarikoski, S., Niemi, J., Kousa, A., Ježek, I., Močnik, G., Carbone, S., Kuuluvainen, H.,
697 Rönkkö, T., Hillamo, R., Pirjola, L., 2016. Chemical and physical characterization of traffic
698 particles in four different highway environments in the Helsinki metropolitan area.
699 Atmospheric, Chemistry and Physics 16, 5497–5512. https://doi.org/10.5194/acp-16-5497-
700 2016
701 Etyemezian, V., Kuhns, H., Gillies, J., Green, M., Pitchford, M., Watson, J., 2003. Vehicle-based road
702 dust emission measurement: I—methods and calibration. Atmospheric Environment 37,
703 4559–4571. https://doi.org/10.1016/S1352-2310(03)00528-4
704 European Environment Agency, 2015. The European environment — state and outlook 2015 [WWW
705 Document]. European Environment Agency. URL https://www.eea.europa.eu/soer (accessed
706 5.14.19).
707 Foitzik, M.-J., Unrau, H.-J., Gauterin, F., Dörnhöfer, J., Koch, T., 2018. Investigation of ultra fine
708 particulate matter emission of rubber tires. Wear 394–395, 87–95.
709 https://doi.org/10.1016/j.wear.2017.09.023
710 Garg, B.D., Cadle, S.H., Mulawa, P.A., Groblicki, P.J., Laroo, C., Parr, G.A., 2000. Brake Wear
711 Particulate Matter Emissions. Environ. Sci. Technol. 34, 4463–4469.
712 https://doi.org/10.1021/es001108h
713 Geiser, M., Kreyling, W.G., 2010. Deposition and biokinetics of inhaled nanoparticles. Particle and
714 Fibre Toxicology 7, 2. https://doi.org/10.1186/1743-8977-7-2
715 Gietl, J.K., Lawrence, R., Thorpe, A.J., Harrison, R.M., 2010. Identification of brake wear particles and
716 derivation of a quantitative tracer for brake dust at a major road. Atmospheric Environment
717 44, 141–146. https://doi.org/10.1016/j.atmosenv.2009.10.016
718 Grigoratos, T., Gustafsson, M., Eriksson, O., Martini, G., 2018. Experimental investigation of tread
719 wear and particle emission from tyres with different treadwear marking. Atmospheric
720 Environment 182, 200–212. https://doi.org/10.1016/j.atmosenv.2018.03.049
721 Grigoratos, T., Martini, G., 2015. Brake wear particle emissions: a review. Environ Sci Pollut Res Int
722 22, 2491–2504. https://doi.org/10.1007/s11356-014-3696-8
723 Grigoratos, T., Martini, G., 2014. Non-exhaust traffic related emissions – Brake and tyre wear PM (JRC
724 SCIENCE AND POLICY REPORT), European Commission.
725 Gustafsson, M., Blomqvist, G., Gudmundsson, A., Dahl, A., Swietlicki, E., Bohgard, M., Lindbom, J.,
726 Ljungman, A., 2008. Properties and toxicological effects of particles from the interaction
727 between tyres, road pavement and winter traction material. Science of The Total
728 Environment 393, 226–240. https://doi.org/10.1016/j.scitotenv.2007.12.030
729 Hagino, H., Oyama, M., Sasaki, S., 2016. Laboratory testing of airborne brake wear particle emissions
730 using a dynamometer system under urban city driving cycles. Atmospheric Environment 131,
731 269–278. https://doi.org/10.1016/j.atmosenv.2016.02.014
732 Hagino, H., Oyama, M., Sasaki, S., 2015. Airborne brake wear particle emission due to braking and
733 accelerating. Wear 334–335, 44–48. https://doi.org/10.1016/j.wear.2015.04.012

734 Harrison, R.M., Jones, A.M., Gietl, J., Yin, J., Green, D.C., 2012. Estimation of the Contributions of
735 Brake Dust, Tire Wear, and Resuspension to Nonexhaust Traffic Particles Derived from
736 Atmospheric Measurements. Environmental Science & Technology 46, 6523–6529.
737 https://doi.org/10.1021/es300894r
738 Harrison, Yin, J., Mark, D., Stedman, J., Appleby, R.S., Booker, J., Moorcroft, S., 2001. Studies of the
739 coarse particle (2.5–10μm) component in UK urban atmospheres. Atmospheric Environment
740 35, 3667–3679. https://doi.org/10.1016/S1352-2310(00)00526-4
741 Hulskotte, J.H.J., Roskam, G.D., Denier van der Gon, H.A.C., 2014. Elemental composition of current
742 automotive braking materials and derived air emission factors. Atmospheric Environment 99,
743 436–445. https://doi.org/10.1016/j.atmosenv.2014.10.007
744 Hussein, T., Johansson, C., Karlsson, H., Hansson, H.-C., 2008. Factors affecting non-tailpipe aerosol
745 particle emissions from paved roads: On-road measurements in Stockholm, Sweden.
746 Atmospheric Environment 42, 688–702. https://doi.org/10.1016/j.atmosenv.2007.09.064
747 Iijima, A., Sato, K., Yano, K., Kato, M., Kozawa, K., Furuta, N., 2008. Emission factor for antimony in
748 brake abrasion dusts as one of the major atmospheric antimony sources. Environmental
749 Science & Technology 42, 2937–2942.
750 Iijima, A., Sato, K., Yano, K., Tago, H., Kato, M., Kimura, H., Furuta, N., 2007. Particle size and
751 composition distribution analysis of automotive brake abrasion dusts for the evaluation of
752 antimony sources of airborne particulate matter. Atmospheric Environment 41, 4908–4919.
753 https://doi.org/10.1016/j.atmosenv.2007.02.005
754 Jeong, C.-H., Evans, G.J., Healy, R.M., Jadidian, P., Wentzell, J., Liggio, J., Brook, J.R., 2015. Rapid
755 physical and chemical transformation of traffic-related atmospheric particles near a highway.
756 Atmospheric Pollution Research 6, 662–672. https://doi.org/10.5094/APR.2015.075
757 Jeong, C.-H., Wang, J.M., Hilker, N., Debosz, J., Sofowote, U., Su, Y., Noble, M., Healy, R.M., Munoz,
758 T., Dabek-Zlotorzynska, E., Celo, V., White, L., Audette, C., Herod, D., Evans, G.J., 2019.
759 Temporal and spatial variability of traffic-related PM2.5 sources: Comparison of exhaust and
760 non-exhaust emissions. Atmospheric Environment 198, 55–69.
761 https://doi.org/10.1016/j.atmosenv.2018.10.038
762 Khardi, S., Nuel, A., 2017. Development of Braking Profiles generating High Rates of Non-exhaust
763 Particle Emissions of Vehicles. Journal of Earth Sciences and Geotechnical Engineering,
764 Special Issue: Transport and Air Pollution, Part 2 7, 89–98.
765 Kim, G., Lee, S., 2018. Characteristics of Tire Wear Particles Generated by a Tire Simulator under
766 Various Driving Conditions. Environ. Sci. Technol. 52, 12153–12161.
767 https://doi.org/10.1021/acs.est.8b03459
768 Kousoulidou, M., Ntziachristos, L., Mellios, G., Samaras, Z., 2008. Road-transport emission projections
769 to 2020 in European urban environments. Atmospheric Environment 42, 7465–7475.
770 https://doi.org/10.1016/j.atmosenv.2008.06.002
771 Kwak, J., Kim, H., Lee, J., Lee, S., 2013. Characterization of non-exhaust coarse and fine particles from
772 on-road driving and laboratory measurements. The Science of the Total Environment 458–
773 460, 273–282. https://doi.org/10.1016/j.scitotenv.2013.04.040
774 Kwak, J., Lee, Sunyoup, Lee, Seokhwan, 2014. On-road and laboratory investigations on non-exhaust
775 ultrafine particles from the interaction between the tire and road pavement under braking
776 conditions. Atmospheric Environment 97, 195–205.
777 https://doi.org/10.1016/j.atmosenv.2014.08.014
778 Lawrence, S., Sokhi, R., Ravindra, K., 2016. Quantification of vehicle fleet PM10 particulate matter
779 emission factors from exhaust and non-exhaust sources using tunnel measurement
780 techniques. Environmental Pollution 210, 419–428.
781 https://doi.org/10.1016/j.envpol.2016.01.011
782 Lee, S., Kwak, J., Kim, H., Lee, J., 2013. Properties of roadway particles from interaction between the
783 tire and road pavement. International Journal of Automotive Technology 14, 163–173.
784 https://doi.org/10.1007/s12239-013-0018-y

785 Leskinen, J., Joutsensaari, J., Lyyränen, J., Koivisto, J., Ruusunen, J., Järvelä, M., Tuomi, T., Hämeri, K.,
786 Auvinen, A., Jokiniemi, J., 2012. Comparison of nanoparticle measurement instruments for
787 occupational health applications. J Nanopart Res 14, 718. https://doi.org/10.1007/s11051-
788 012-0718-7
789 Li, X., Dallmann, T.R., May, A.A., Stanier, C.O., Grieshop, A.P., Lipsky, E.M., Robinson, A.L., Presto,
790 A.A., 2018. Size distribution of vehicle emitted primary particles measured in a traffic tunnel.
791 Atmospheric Environment 191, 9–18. https://doi.org/10.1016/j.atmosenv.2018.07.052
792 Liati, A., Schreiber, D., Lugovyy, D., Gramstat, S., Dimopoulos Eggenschwiler, P., 2019. Airborne
793 particulate matter emissions from vehicle brakes in micro- and nano-scales: Morphology and
794 chemistry by electron microscopy. Atmospheric Environment 212, 281–289.
795 https://doi.org/10.1016/j.atmosenv.2019.05.037
796 Lindgren, Å., 1996. Asphalt wear and pollution transport. Science of The Total Environment, Highway
797 and Urban Pollution 189–190, 281–286. https://doi.org/10.1016/0048-9697(96)05220-5
798 Lowne, R.W., 1970. The effect of road surface texture on tyre wear. Wear 15, 57–70.
799 https://doi.org/10.1016/0043-1648(70)90186-9
800 Lu, T., Cheung, C.S., Huang, Z., 2012. Size-Resolved Volatility, Morphology, Nanostructure, and
801 Oxidation Characteristics of Diesel Particulate. Energy Fuels 26, 6168–6176.
802 https://doi.org/10.1021/ef3010527
803 Mathissen, M., Scheer, V., Vogt, R., Benter, T., 2011. Investigation on the potential generation of
804 ultrafine particles from the tire–road interface. Atmospheric Environment 45, 6172–6179.
805 https://doi.org/10.1016/j.atmosenv.2011.08.032
806 MSR, M.S.R., 2019. Automotive Brake Pads Market Share | Industry Size Report 2019-2025 (Research
807 report).
808 Namgung, H.-G., Kim, J.B., Kim, M.-S., Kim, M., Park, S., Woo, S.-H., Bae, G.-N., Park, D., Kwon, S.-B.,
809 2017. Size distribution analysis of airborne wear particles released by subway brake system.
810 Wear 372–373, 169–176. https://doi.org/10.1016/j.wear.2016.12.026
811 Namgung, H.-G., Kim, J.-B., Woo, S.-H., Park, S., Kim, M., Kim, M.-S., Bae, G.-N., Park, D., Kwon, S.-B.,
812 2016. Generation of Nanoparticles from Friction between Railway Brake Disks and Pads.
813 Environmental Science & Technology 50, 3453–3461.
814 https://doi.org/10.1021/acs.est.5b06252
815 Nosko, O., Olofsson, U., 2017. Quantification of ultrafine airborne particulate matter generated by
816 the wear of car brake materials. Wear 374–375, 92–96.
817 https://doi.org/10.1016/j.wear.2017.01.003
818 Oakes, M.M., Burke, J.M., Norris, G.A., Kovalcik, K.D., Pancras, J.P., Landis, M.S., 2016. Near-road
819 enhancement and solubility of fine and coarse particulate matter trace elements near a
820 major interstate in Detroit, Michigan. Atmospheric Environment 145, 213–224.
821 https://doi.org/10.1016/j.atmosenv.2016.09.034
822 Padoan, E., Amato, F., 2018. Chapter 2 - Vehicle Non-Exhaust Emissions: Impact on Air Quality, in:
823 Amato, F. (Ed.), Non-Exhaust Emissions. Academic Press, pp. 21–65.
824 https://doi.org/10.1016/B978-0-12-811770-5.00002-9
825 Pant, P., Harrison, R.M., 2013. Estimation of the contribution of road traffic emissions to particulate
826 matter concentrations from field measurements: A review. Atmospheric Environment 77,
827 78–97. https://doi.org/10.1016/j.atmosenv.2013.04.028
828 Park, I., Kim, H., Lee, S., 2018. Characteristics of tire wear particles generated in a laboratory
829 simulation of tire/road contact conditions. Journal of Aerosol Science 124, 30–40.
830 https://doi.org/10.1016/j.jaerosci.2018.07.005
831 Pelkmans, L., Debal, P., 2006. Comparison of on-road emissions with emissions measured on chassis
832 dynamometer test cycles. Transportation Research Part D: Transport and Environment 11,
833 233–241. https://doi.org/10.1016/j.trd.2006.04.001
834 Pirjola, L., Johansson, C., Kupiainen, K., Stojiljkovic, A., Karlsson, H., Hussein, T., 2010. Road dust
835 emissions from paved roads measured using different mobile systems. Journal of the Air &

836 Waste Management Association 60, 1422–1433. https://doi.org/10.3155/1047-
837 3289.60.12.1422
838 Pope, C.A., Burnett, R.T., Thun, M.J., Calle, E.E., Krewski, D., Ito, K., Thurston, G.D., 2002. Lung cancer,
839 cardiopulmonary mortality, and long-term exposure to fine particulate air pollution. JAMA
840 287, 1132–1141.
841 Querol, X., Alastuey, A., Ruiz, C.R., Artiñano, B., Hansson, H.C., Harrison, R.M., Buringh, E., ten Brink,
842 H.M., Lutz, M., Bruckmann, P., Straehl, P., Schneider, J., 2004. Speciation and origin of PM10
843 and PM2.5 in selected European cities. Atmospheric Environment, Contains Special Issue
844 section on Measuring the composition of Particulate Matter in the EU 38, 6547–6555.
845 https://doi.org/10.1016/j.atmosenv.2004.08.037
846 Sanders, P.G., Xu, N., Dalka, T.M., Maricq, M.M., 2003. Airborne Brake Wear Debris: Size
847 Distributions, Composition, and a Comparison of Dynamometer and Vehicle Tests.
848 Environmental Science & Technology 37, 4060–4069. https://doi.org/10.1021/es034145s
849 Sanderson, P., Su, S.S., Chang, I.T.H., Delgado Saborit, J.M., Kepaptsoglou, D.M., Weber, R.J.M.,
850 Harrison, R.M., 2016. Characterisation of iron-rich atmospheric submicrometre particles in
851 the roadside environment. Atmospheric Environment 140, 167–175.
852 https://doi.org/10.1016/j.atmosenv.2016.05.040
853 Sjödin, Å., Ferm, M., Björk, A., Rahmberg, M., Gudmundsson, A., Swietlicki, E., Johansson, C.,
854 Gustafsson, M., Blomqvist, G., 2010. Wear particles from road traffic - a field, laboratory and
855 modeling study. IVL Swedish Environment Research Institute Ltd. 101.
856 Stone, V., Miller, M.R., Clift, M.J.D., Elder, A., Mills, N.L., Møller, P., Schins, R.P.F., Vogel, U., Kreyling,
857 W.G., Alstrup Jensen, K., Kuhlbusch, T.A.J., Schwarze, P.E., Hoet, P., Pietroiusti, A., De
858 Vizcaya-Ruiz, A., Baeza-Squiban, A., Teixeira, J.P., Tran, C.L., Cassee, F.R., 2017.
859 Nanomaterials Versus Ambient Ultrafine Particles: An Opportunity to Exchange Toxicology
860 Knowledge. Environ. Health Perspect. 125, 106002. https://doi.org/10.1289/EHP424
861 Sun, Q., Hong, X., Wold, L.E., 2010. Cardiovascular effects of ambient particulate air pollution
862 exposure. Circulation 121, 2755–2765.
863 https://doi.org/10.1161/CIRCULATIONAHA.109.893461
864 Thorpe, A., Harrison, R.M., 2008. Sources and properties of non-exhaust particulate matter from road
865 traffic: A review. Science of the Total Environment 400, 270–282.
866 https://doi.org/10.1016/j.scitotenv.2008.06.007
867 Valavanidis, A., Fiotakis, K., Vlachogianni, T., 2008. Airborne particulate matter and human health:
868 toxicological assessment and importance of size and composition of particles for oxidative
869 damage and carcinogenic mechanisms. J Environ Sci Health C Environ Carcinog Ecotoxicol Rev
870 26, 339–362. https://doi.org/10.1080/10590500802494538
871 Van der Gon, H.A.C.D., Gerlofs-Nijland, M.E., Gehrig, R., Gustafsson, M., Janssen, N., Harrison, R.M.,
872 Hulskotte, J., Johansson, C., Jozwicka, M., Keuken, M., Krijgsheld, K., Ntziachristos, L.,
873 Riediker, M., Cassee, F.R., 2013. The policy relevance of wear emissions from road transport,
874 now and in the future--an international workshop report and consensus statement. Journal
875 of the Air & Waste Management Association 63, 136–149.
876 Virtanen, A., Joutsensaari, J., Koop, T., Kannosto, J., Yli-Pirilä, P., Leskinen, J., Mäkelä, J.M.,
877 Holopainen, J.K., Pöschl, U., Kulmala, M., Worsnop, D.R., Laaksonen, A., 2010. An amorphous
878 solid state of biogenic secondary organic aerosol particles. Nature 467, 824–827.
879 https://doi.org/10.1038/nature09455
880 Von Uexküll, O., Skerfving, S., Doyle, R., Braungart, M., 2005. Antimony in brake pads-a carcinogenic
881 component? Journal of Cleaner Production 13, 19–31.
882 https://doi.org/10.1016/j.jclepro.2003.10.008
883 Vouitsis, E., Ntziachristos, L., Pistikopoulos, P., Samaras, Z., Chrysikou, L., Samara, C., Papadimitriou,
884 C., Samaras, P., Sakellaropoulos, G., 2009. An investigation on the physical, chemical and
885 ecotoxicological characteristics of particulate matter emitted from light-duty vehicles.
886 Environmental Pollution 157, 2320–2327. https://doi.org/10.1016/j.envpol.2009.03.028

887 Wahlström, J., Olander, L., Olofsson, U., 2010a. Size, Shape, and Elemental Composition of Airborne
888 Wear Particles from Disc Brake Materials. Tribol Lett 38, 15–24.
889 https://doi.org/10.1007/s11249-009-9564-x
890 Wahlström, J., Söderberg, A., Olander, L., Jansson, A., Olofsson, U., 2010b. A pin-on-disc simulation of
891 airborne wear particles from disc brakes. Wear 268, 763–769.
892 https://doi.org/10.1016/j.wear.2009.11.014
893 Weinbruch, S., Worringen, A., Ebert, M., Scheuvens, D., Kandler, K., Pfeffer, U., Bruckmann, P., 2014.
894 A quantitative estimation of the exhaust, abrasion and resuspension components of
895 particulate traffic emissions using electron microscopy. Atmospheric Environment 99, 175–
896 182. https://doi.org/10.1016/j.atmosenv.2014.09.075
897 Zhang, Q., Ning, Z., Shen, Z., Li, G., Zhang, J., Lei, Y., Xu, H., Sun, J., Zhang, L., Westerdahl, D., Gali,
898 N.K., Gong, X., 2017. Variations of aerosol size distribution, chemical composition and optical
899 properties from roadside to ambient environment: A case study in Hong Kong, China.
900 Atmospheric Environment 166, 234–243. https://doi.org/10.1016/j.atmosenv.2017.07.030
901 Zhang, X., Craft, E., Zhang, K., 2017. Characterizing spatial variability of air pollution from vehicle
902 traffic around the Houston Ship Channel area. Atmospheric Environment 161, 167–175.
903 https://doi.org/10.1016/j.atmosenv.2017.04.032
904

List of Tables

	Brake Wear (BW) particles							Tire-Road Contact (TRC) particles							
	Accumulation mode (A) (n=612)			Coarse mode (C) (n=195)				Accumulation mode (A) (n=274)			Coarse mode (C) (n=360)				
	BW-A1	BW-A2	BW-A3	BW-C1	BW-C2	BW-C3	BW-C4	TRC-A1	TRC-A2	TRC-A3	TRC-C1	TRC-C2	TRC-C3	TRC-C4	TRC-C5
	P= 29%	P= 25%	P= 47%	P= 5%	P= 2%	P= 76%	P= 17%	P= 18%	P= 64%	P= 19%	P= 21%	P= 6%	P= 19%	P= 14%	P= 40%
Dm	0.16	0.21	0.52	2.16	2.62	2.61	2.58	0.64	0.37	0.87	1.95	1.42	1.76	1.78	1.48
C	76.8	64.1	41.5	54.7	18.1	21.1	17.1	39.9	69.6	37.2	33.9	47.7	29.6	40.1	45.4
N	2.3											15.2			2.9
O	18.1	22.4	28.5	32.6	35.7	29.7	26.6	43.9	27.2	29.1	45.0	30.8	29.8	39.7	23.1
Na											1.4		1.5	1.3	14.1
Mg														1.4	
Al		0.8	1.0		17.1	1.8		2.7			4.2			1.9	
Si		1.1	1.3	1.2		1.9	1.5	9.5	1.4	1.3	11.8	1.3	1.1	4.8	
S	1.8			1.8											
Cl															12.0
K											1.7				
Ca														4.6	
Fe		10.3	23.4	8.7	25.2	38.3	53.8	1.3		31.1		2.5	35.5	3.9	
Cu		1.2	3.6	0.8	3.2	6.4									

Table 1: Mean diameter (Dm, in µm) and mean elemental composition (wt. %) for particles emitted from brake wear and tire-road contact. The number of particles analyzed (n) by SEM-EDX and the relative proportion (P) of the various particle types are indicated for each size mode. Only those elements with a mean concentration of at least 0.8% are reported.

List of figures

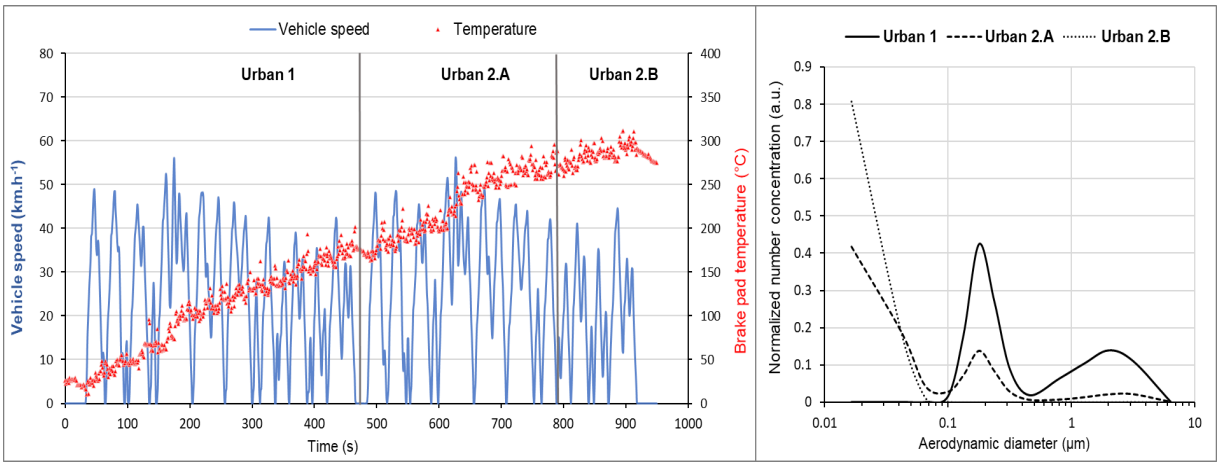

Figure 1: Evolution of brake pad temperature during two successive urban profiles (left) and mean number size distributions of BWP after the removal of atmospheric background for the corresponding profile periods (right)

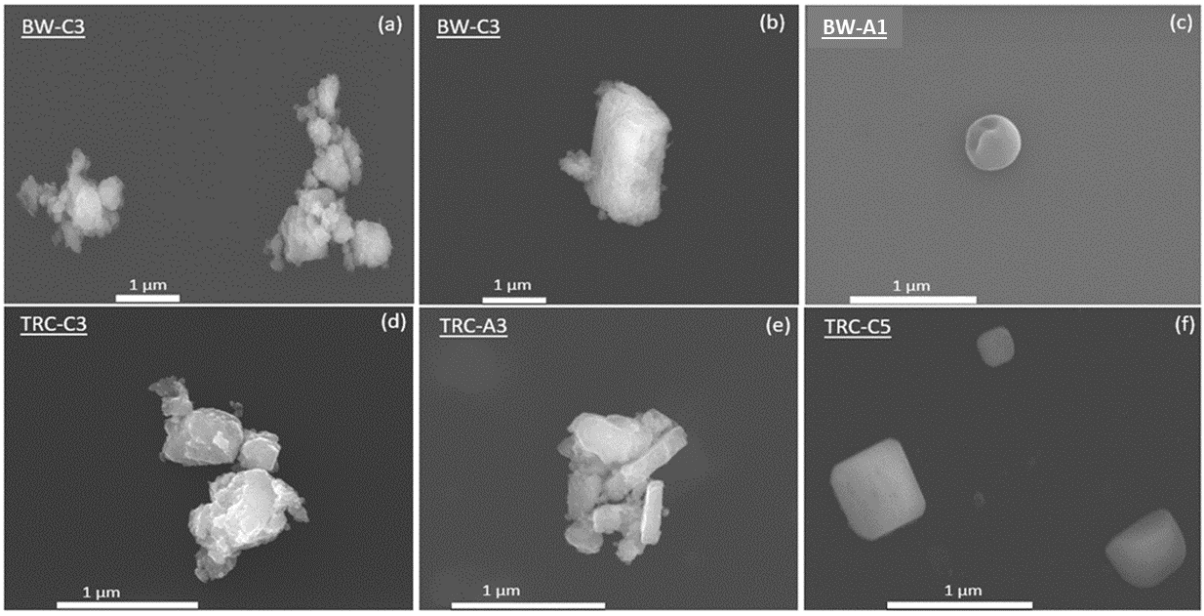

Figure 2: Typical morphologies of brake wear (BW) and tire-road contact (TRC) particles: agglomerated (a), flaky (b), spherical (c), agglomerated (d), agglomerated (e), angular (f). The identification of these particles (top left of each SEM-EDX image) corresponds to the particle types in Table 1.

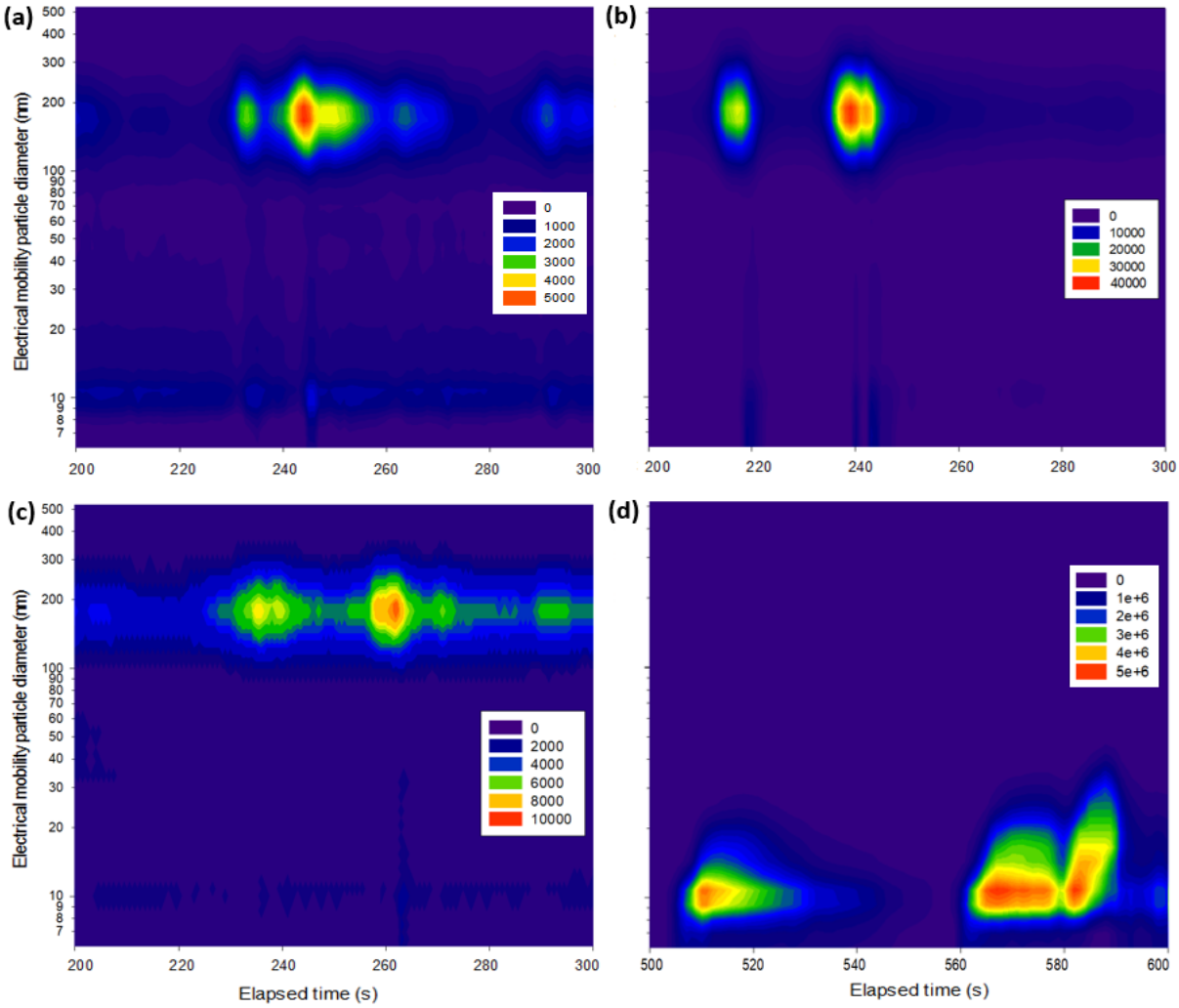

Figure 3: Temporal evolution of the size distribution of BWP emissions for the (a) urban, (b) suburban, (c) highway braking profiles 200 s after the profile starting point, and (d) for the highway braking profile 500 s after the starting point. All concentrations are given in #.cm^{-3}.

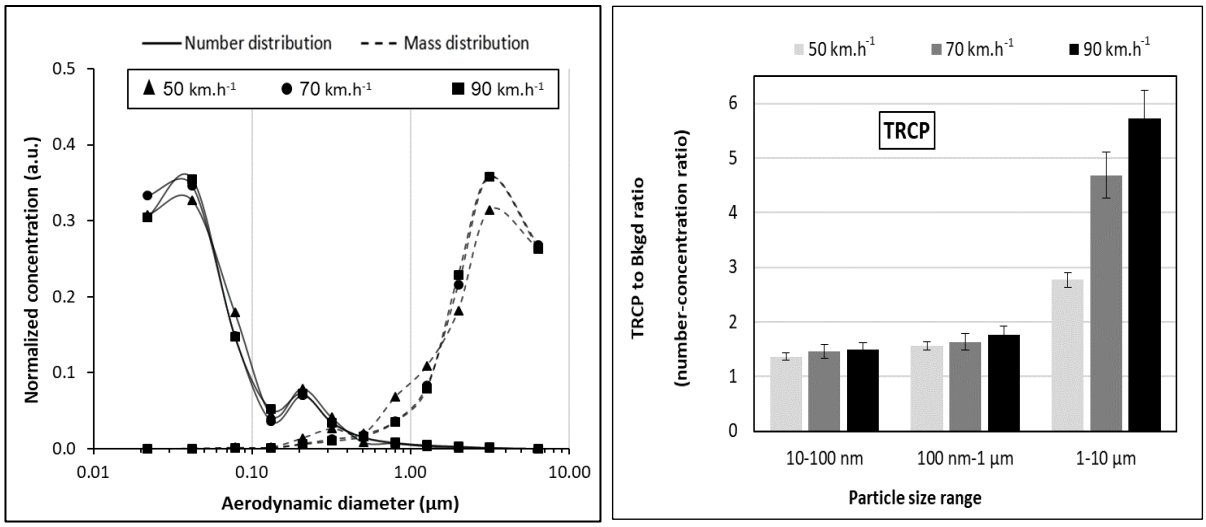

935

936 *Figure 4: Normalized number and mass size distributions of TRCP after background removal (left) and TRCP-to-background*
937 *(Bkgd) concentration ratios (right) in considering the 0.01-10 µm particle size range (aerodynamic diameters). The error bars*
938 *account for standard errors calculated over the dataset from five successive tests.*

939

940

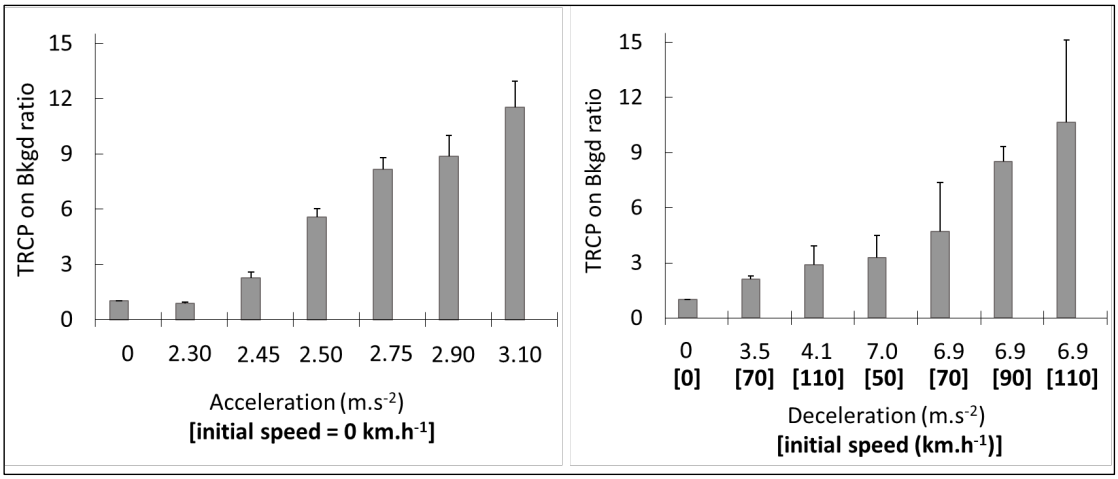

941

942 *Figure 5: Evolution of TRCP-to-background (Bkgd) concentration ratios in considering the 0.35-10µm size range of optical*
943 *diameter for increased acceleration (a) or deceleration (b) powers. The error bars account for standard errors calculated*
944 *over the dataset from five successive tests.*

945

946

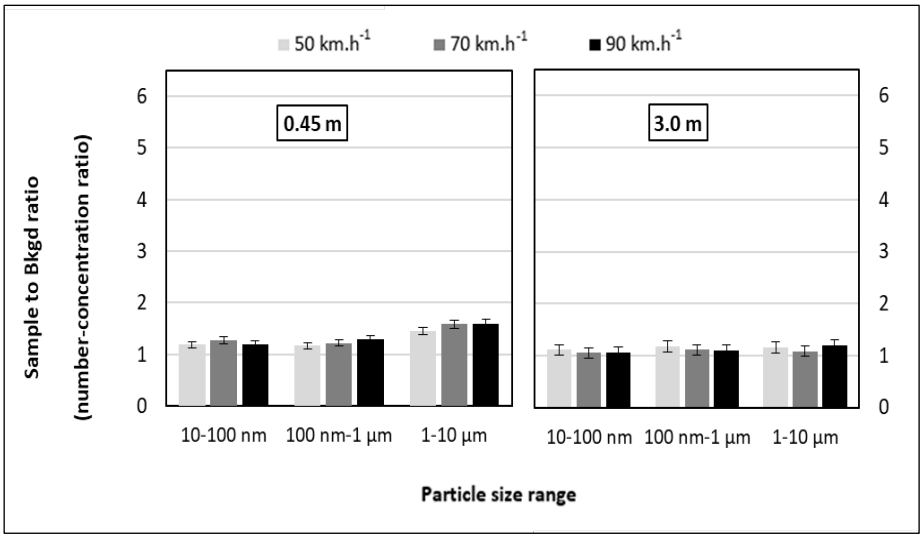

947

948 *Figure 6: Sample-to-background (Bkgd) concentration ratios measured at the edge of the test track at an increasing distance*
949 *from the driving lane (0.45 and 3.0 m) in considering the 0.01-10 µm particle size range (aerodynamic diameters). The error*
950 *bars account for standard errors calculated over the dataset from five successive tests.*

951

952

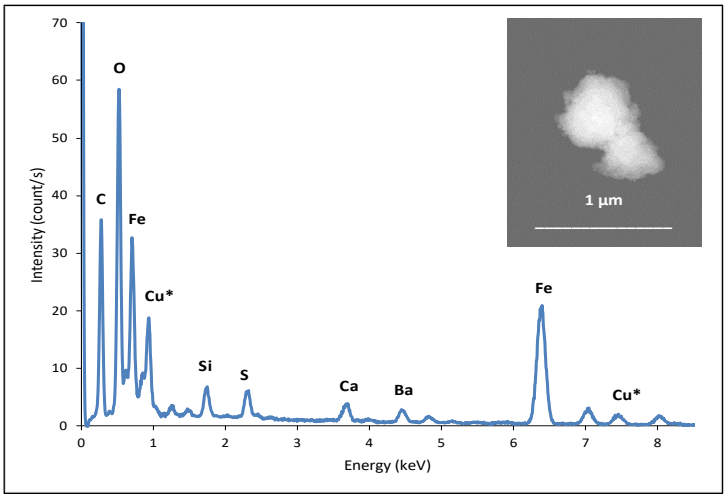

953

954 *Figure 7:* SEM image and EDX spectrum for a typical Fe-containing particle collected along the roadside and classified in the
955 FeR-A1 cluster (*: Cu is from the grid holder)

956

Supplementary information

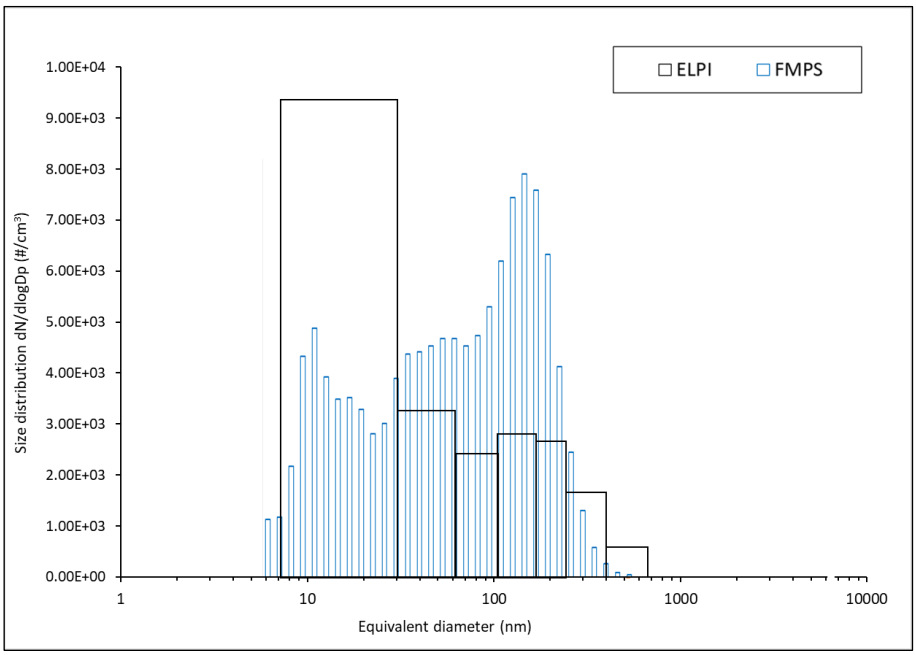

Figure S1: Example of comparison of aerodynamic diameters measured by ELPI (in black) with mobility diameters measured by FMPS (in blue). The two main modes are well coinciding for the two measurements although there is an apparent overestimation of particle counts in the nano-size range of ELPI, and therefore an underestimation of larger ones, which was already been reported and attributed to particle bounce (Leskinen et al., 2012; Virtanen et al., 2010).

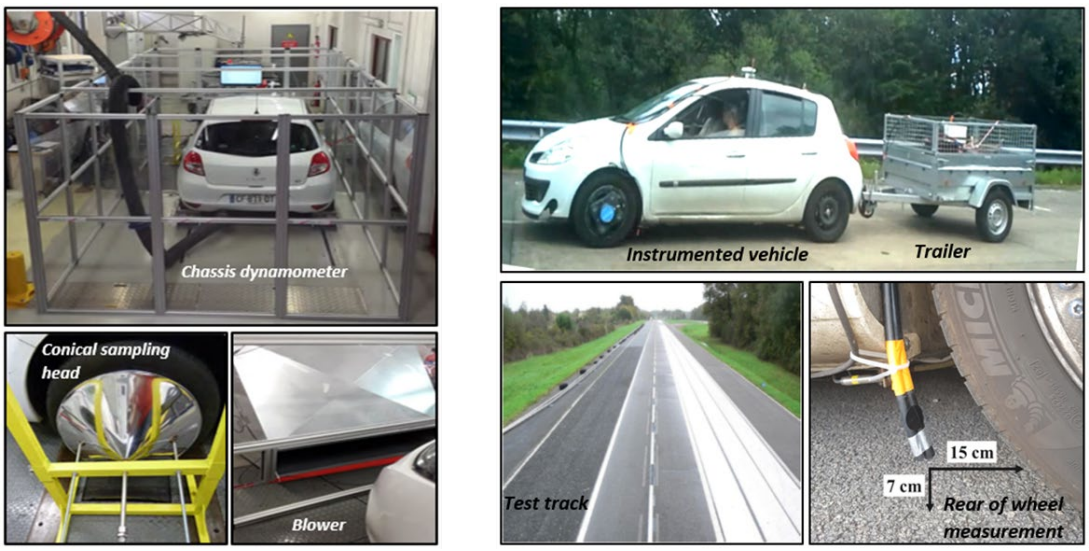

Figure S2: Photograph of the laboratory test on the chassis dynamometer (left) and measurements conducted on the test track using a trailer loaded with instruments (right)

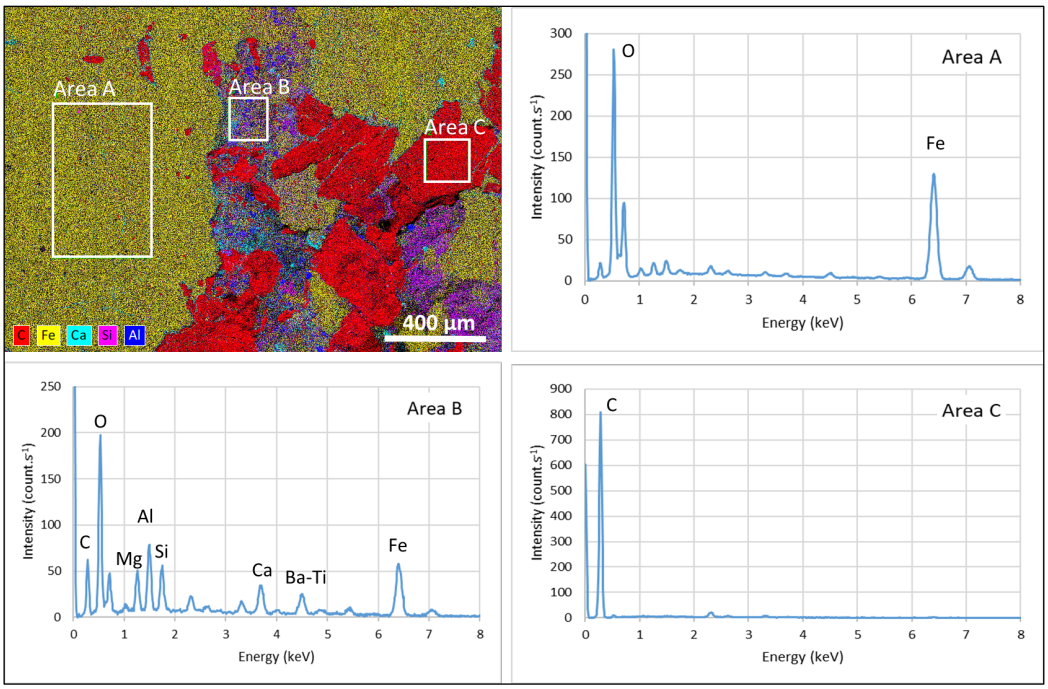

969

970 *Figure S3: Elemental map of a brake pad surface for a semi-metallic pad and EDX spectra for the corresponding areas (A, B*
971 *and C)*

972

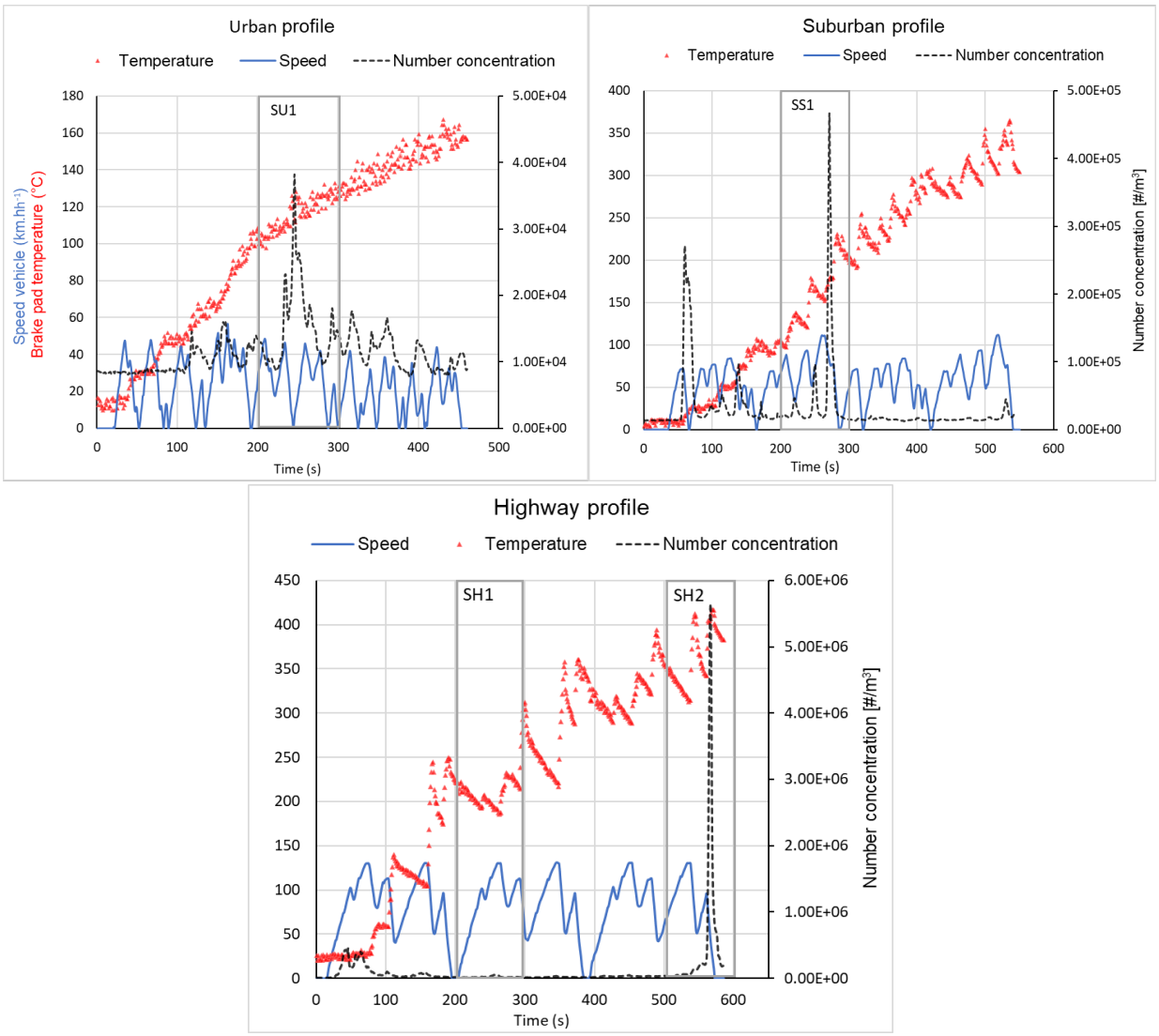

Figure S4: Brake pad temperature evolution (in red) and PM concentration (black) vs. vehicle speed (blue) for three braking profiles: urban, suburban, and highway. The gray areas correspond to the temporal evolutions of the BWP size distributions presented in Figure 3.

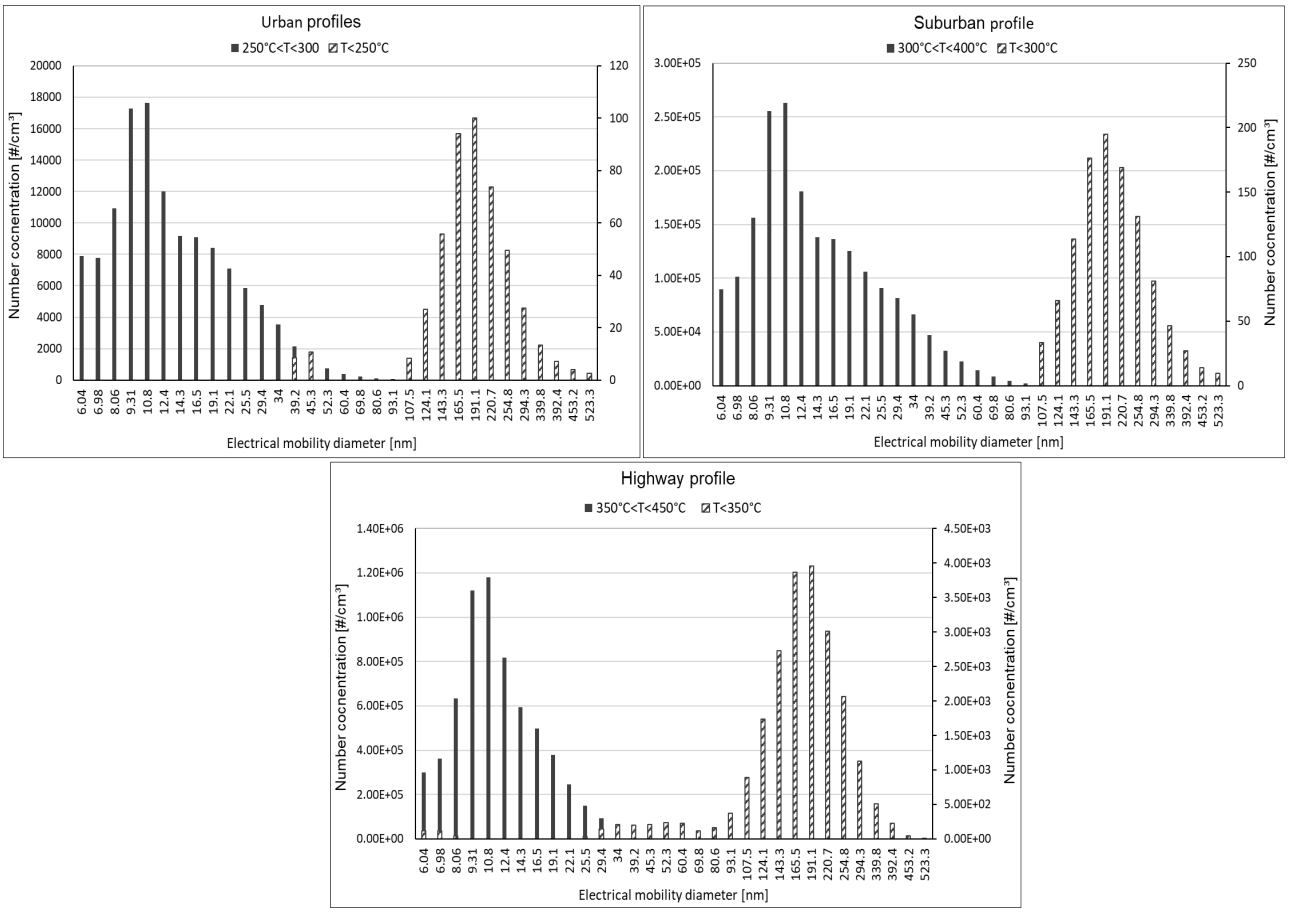

Figure S5: Average number size distribution (after removal of the atmospheric background) of BWP emitted during urban, suburban and highway profiles vs. brake pad temperature

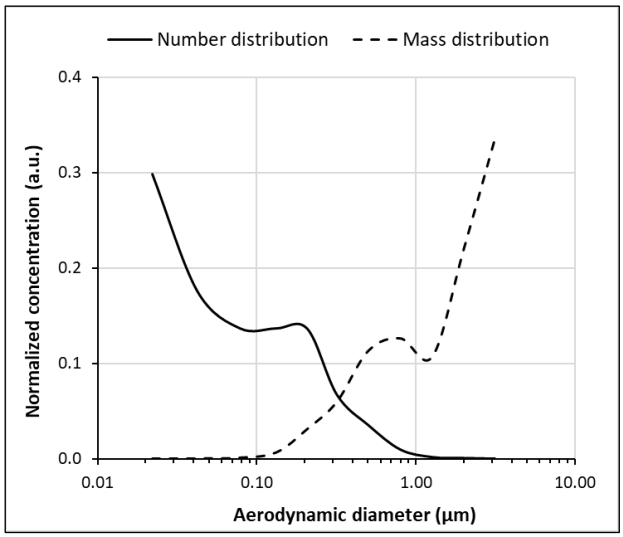

Figure S6: Normalized number and mass size distributions of ambient particles along the roadside

Vehicle speed	50 km/h	90 km/h	110 km/h
U_0 (m/s)	1.39	2.5	3.06
U (m/s)	6.632	6.632	6.632
η for particle diameter of 1 µm	1.000	1.000	1.000
η for particle diameter of 5 µm	1.000	0.995	0.988
η for particle diameter of 10 µm	0.996	0.949	0.908

Table S 1 : Aspiration efficiency for particles in the range 1-10µm for different simulated vehicle speeds. Considering the experimental configuration, the air flow velocity in the free-stream (U0) at the sampling head is estimated to be 10 times lower than the simulated vehicle speed due to air dilution.

Vehicle speed	50 km/h	70 km/h	90 km/h
U_0 (m/s)	3.345	4.344	5.345
U (m/s)	3.316	3.316	3.316
η for particle diameter of 1 µm	0.997	0.994	0.989
η for particle diameter of 5 µm	0.928	0.892	0.867
η for particle diameter of 10 µm	0.715	0.639	0.603

Table S 2: Aspiration efficiency for particles in the range 1-10µm for different vehicle speeds. The flow velocity in the free-stream (U0) was evaluated considering the relation between the vehicle speed and the flow velocity behind the front tire established by (Kwak et al., 2013).

	Fe-containing particles along the Roadside (FeR)				
	Accumulation mode (A) (n=51)		Coarse mode (C) (n=442)		
	FeR-A1	FeR-A2	FeR-C1	FeR-C2	FeR-C3
	P=56%	P=44%	P=58%	P=23%	P=19%
Dm	0.87	0.65	3.50	2.40	2.15
C	23.1	37.1	33.8	22.1	17.8
N					7.6
O	29.5	37.8	30.8	45.6	46.0
Na				1.3	6.5
Mg				0.9	1.1
Al				2.5	
Si	1.1	4.13	1.0	6.4	1.4
S			1.0	1.6	1.4
Ca		2.5		3.4	4.3
Fe	45.6	16.1	31.0	15.3	13.1

Table S3: Mean diameter (Dm, in µm) and mean elemental composition (wt. %) of Fe-containing particles collected along the roadside for the PM1-10 and PM0, 1-1 µm stages (classification by means of clustering analysis from 51 coarse and 442 fine particles analyzed with SEM-EDX). The number of particles (n) analyzed by SEM-EDX and the relative proportion (P) of the various particle types are indicated for each size mode. Only those elements with a mean concentration of at least 0.8% are reported.